Ionic fragmentation of K-shell excited and ionized CO

A. P. Hitchcock,* P. Lablanquie, P. Morin,† E. Lizon A Lugrin,† M. Simon,† P. Thiry, and I. Nenner†

Laboratoire pour l'Utilisation du Rayonnement Electromagnétique, Université de Paris Sud, 91405, Orsay Cédex, France

(Received 28 August 1987)

Quantitative ion yields from photoionization of gaseous CO have been measured with time-of-flight mass spectrometry and photoion-photoion coincidence techniques using synchrotron radiation from 270 to 360 eV and from 515 to 615 eV, in the region of C 1s and O 1s excitation and ionization. Dissociative multiple-ionization efficiencies, ion-branching ratios, and the relative yields of all possible ionization reactions are derived. The distributions of kinetic energies released to the $(C^+ + O^+)$ and $(C^{2+} + O^+)$ pairs are measured. Very large contributions of symmetric dissociative double ionization producing C^+ and O^+ are found, even in the region of the $1s \rightarrow \pi^*$ resonances. The results are discussed in the context of the autoionization and Auger electron spectroscopy of core-excited CO and with the aid of recent calculations of the potential curves of CO^{2+}. The relationship between the present results and those for photon-stimulated desorption following core excitation and ionization of solid and chemisorbed CO is explored.

I. INTRODUCTION

The possibility of selective bond breaking in a polyatomic molecule through photodissociation involving core-excited states is receiving considerable attention at present.[1-6] In principle one might suppose that selective fragmentation could result from preferential breaking of the bonds closest to the core-excited atom, possibly assisted by population of a localized antibonding molecular orbital. In practice fragmentation frequently occurs at bonds distant from the core-excited atom[7,8] and thus the selectivity is considerably less than expected. The photoionization dynamics, in particular the relaxation of the core-hole state to dissociative, multiply ionized valence-hole states, determines the details of the fragmentation reactions. Furthermore, complications arise when the core-hole relaxation and the dissociation occur on overlapping time scales.[9-13] Both the electronic decay and the ion production must be studied in detail in a number of test cases in order to acquire an understanding of the physical mechanisms and thus to develop means for predicting situations in which selective fragmentation through core excitation can be achieved. As part of this process we have studied the ionic fragmentation of core-excited CO in some detail.

One of the principal models for fragmentation following core ionization of molecules is that of a "Coulomb explosion"[14] in which the charge repulsion in two-hole states produced from the core-hole Auger decay results in two energetic fragment ions. For CO the major process of this type is

$$CO + h\nu \rightarrow C^+ + O^+ .$$

In addition, triple ionization associated with the decay of shake-off states can produce $(C^{2+} + O^+)$ or $(C^+ + O^{2+})$ pairs. We have used photoion-photoion coincidence (PIPICO) techniques[15] to investigate the yields and ion kinetic energy releases involved in these processes in the C 1s and O 1s spectral regions. The derived ion kinetic energies are compared to previous estimates[16-18] and to values predicted from the *ab initio* calculations of the potential curves of CO^{2+} states which lead to $(C^+ + O^+)$ atomic ion limits.[19] The latter comparison helps in identifying which CO^{2+} states and thus $(C^+ + O^+)$ limits are populated in the core-hole relaxation through the observed kinetic energy released to the ion pair.

The electronic relaxation of the core-hole states of CO has been studied in considerable detail recently through electron-electron coincidence techniques,[20,21] through electron spectra recorded at selected photon energies,[1,18,22] and by Auger electron-ion coincidence spectra obtained with broadband photoionization around 300 and 1200 eV.[23] The autoionization spectrum of the C $\underline{1s}\pi^*$ state of CO (287.4 eV) has been interpreted by Freund and Liegener[24] with the aid of Green's-function calculations. A very extensive analysis of the vibrationally resolved features in the photoelectron,[25] x-ray emission,[26] Auger,[9] autoionization,[9] and core-excitation[27,28] spectra has been presented by Correia *et al.*[9] Reference 9 also gives a rather complete summary of earlier inner-shell spectroscopic studies of CO, which are not completely cited here. We have interpreted our quantitative ionic fragmentation measurements with the aid of these results.

There is considerable interest at present in the yields and mechanisms of ion desorption from surfaces following core excitation and ionization by electron impact (ESD) or soft x-ray photoabsorption (PSID). Several PSID studies of CO adsorbed on transition-metal surfaces[29-32] have observed K-shell ion yield spectra with desorption onsets greatly delayed relative to the K-shell absorption spectrum. In the proposed interpretation of these differences Jaeger and Stöhr[29,30] assumed that the O^+ yield of free CO follows the O 1s absorption spec-

trum. This is confirmed in the present work. In addition, improved understanding of photoionization fragmentation in the free molecule assists the determination of the role of the substrate in modifying these processes.

Ionic fragmentation of gaseous CO in the carbon K shell has been studied previously both by $(e,e+\text{ion})$, the electron-ion coincidence simulation of photoionization mass spectrometry (PIMS),[18,33,34] and by synchrotron PIMS using both quadrupole[1,2] and time-of-flight (TOF)[18,35] mass analyzers. However, the C 1s results cover a very restricted energy range while the only measurements of ionic fragmentation following O 1s excitation and ionization of which we are aware are the PIMS at 930 eV (Ref. 16) as well as previously unpublished mass spectra at 534 (Ref. 34) and 550 eV,[34,35] the results of which are quoted in this paper. The O^+ yield from both C 1s and O 1s photoionization of a multilayer solid film of CO has been measured[36] and shows greater similarity to the gas phase absorption than to the surface chemisorbed O^+ yield spectrum. However, differences between the solid film and gas phase ion yield spectra were noted in the C 1s region so the possibility of even greater differences in the O 1s region existed prior to the present study. Our measurements of ionic fragmentation following O 1s photoionization are compared in detail with the PSID of adsorbed CO.[29–32]

This paper is organized as follows. Section II deals with experimental details such as the monochromator, energy scale calibration, flux normalization, the ion time-of-flight spectrometer, and our procedures for collecting mass and ion-ion coincidence spectra. Section III presents our results in detail. Section III A, dealing with the noncoincident measurements, includes a comparison of the true absorption and total ion yield spectra (Sec. III A 1), presentation of the partial ion yields (Sec. III A 2) and branching ratio spectra (Sec. III A 3), in each case comparing our results to earlier work. Section III B deals with the ion-ion coincidence results in two subsections. In the first (III B 1) quantitative ion-pair yields and dissociative multiple-ionization efficiencies are derived, while in the second (III B 2) kinetic energy release distributions are determined from the PIPICO peak shapes. In Sec. III C the partial ion and ion-pair yields are combined to derive the relative contributions of all possible photoionization reactions of CO in the separate excitation and ionization channels. The physics of the electronic processes leading to ionic fragmentation following core ionization (Sec. IV A) and excitation (Sec. IV B) of free CO are then discussed, followed by comparison of our results with those for PSID of surface-adsorbed and solid CO (Sec. IV C). Finally, in Sec. IV D we comment on the possibilities of site- and/or state-selective ionic fragmentation following core excitation and ionization.

II. EXPERIMENTAL

A. The monochromator

The toroidal grating monochromator (TGM) used in these experiments was recently installed on the A62 beam line at the Anneau de Collisions d'Orsay (ACO) storage ring in Orsay. Based on the principles outlined by Himpsel *et al.*,[37] this TGM was designed for high-flux efficiency and medium resolving power ($\lambda/\Delta\lambda \simeq 2500$) in the 200–700 eV photon-energy range, with reasonable performance extending up to 1000 eV. The synchrotron radiation continuum is dispersed using one of three ion-etched, platinum-coated, holographic, toroidal gratings without aberration correction. These are interchangeable under vacuum and have optimum performance ranges of 200–300 eV (800 grooves/mm), 300–450 eV (1200 grooves/mm), and 450–750 eV (1800 grooves/mm). Figure 1 is a schematic of the monochromator in its present configuration. For reasons of overall dimensions and available space, the monochromator is mounted without an entrance slit so that the optical source is defined by the size of the electron bunch in the storage ring. In this situation the resolving power is source-size limited. The measured resolution ($\simeq$0.5 eV at 200 eV, 2 eV at 500 eV, and 3 eV at 700 eV) is compatible with the typical 1-mm dimension of the ACO electron beam. In its future installation on "super ACO" a more conventional mounting will be used (prefocussing toroidal mirror, entrance slit, grating, exit slit, postfocussing toroidal mirror, experiment). This will improve the energy scale stability and allow the resolution to achieve the nominal design performance.

The absence of an entrance slit means that the photon energy scale drifts whenever there are changes in the electron orbit in the storage ring. We frequently observe small shifts ($<$0.5 eV at 300 eV) in the energy scales between spectra recorded during a single fill and larger ones

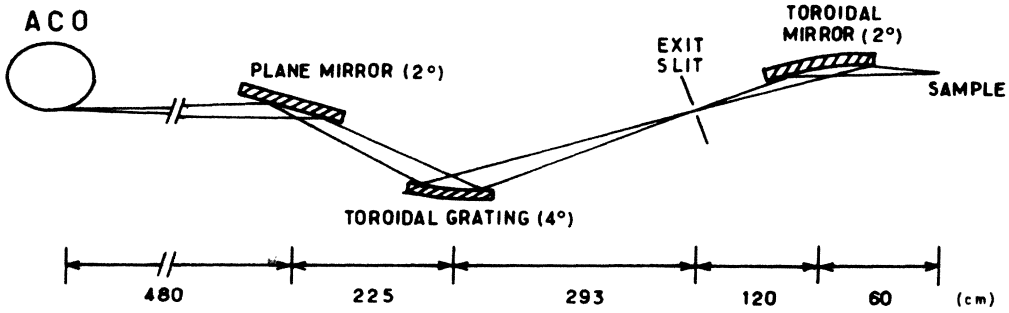

FIG. 1. Schematic of the 10-m TGM monochromator as mounted on line A-62 at the Anneau de Collision d'Orsay (ACO).

(up to 10 eV) between fills. Thus we have normalized each spectrum individually, using either the well-known values for the π^* resonances[38] or, for the Ar flux measurements, the structure in the incident photon flux, which arises from photoabsorption by carbon and oxygen contaminants on the optics. The energies of these latter features are found to be highly reproducible, independent of the gas studied. For calibration we use values of 284.7 eV and 290.0 eV for the two C 1*s* minima and 537.0 eV for the O 1*s* minimum (Fig. 2). The 5.3-eV separation of our two C 1*s* features differs significantly from that of 6.3 eV reported by Arvanitis *et al.*[39] for the BESSY SX-700 monochromator, suggesting that the chemical identity of the carbon contaminant can differ among monochromators.

We have found that simultaneous measurement of the photoionization yield of a Au surface placed in the photoionization chamber ($P \simeq 10^{-5}$–10^{-6} torr) is not an accurate measure of the incident photon flux, particularly in the C 1*s* region (see Fig. 2). It appears that carbon adsorbed on the Au photodiode greatly increases its ionization efficiency above 290 eV. Thus we have measured the incident photon flux from the total ion yield spectrum of Ar. Since the Ar ion yield varies smoothly in the C 1*s* and O 1*s* regions, this allows a correct determination of the structured incident flux, once corrections for the shape of the Ar absorption cross section[40] have been applied. Since the CO and Ar measurements cannot be made simultaneously, we make an additional correction for the smooth decrease in the stored current over the time of each measurement.

A further complication in the O 1*s* region is the presence of some diffuse light, suspected to be primarily of energies less than 200 eV. This stray light distorts our measurements by increasing the CO^+ and CO^{2+} yields, since these are much more abundant at low photon energies. This effect was minimized by recording the O 1*s* data with a 0.4-μm aluminium filter in the light beam. The Al preferentially absorbs the diffuse light and, for example, reduces the CO^+ branching ratio at 550 eV from 0.02 to 0.01.

B. Ion yields and photoion-photoion coincidences (PIPICO)

The apparatus and time-of-flight (TOF) techniques used to obtain both mass spectra and ion-ion coincidence (PIPICO) signals have been described elsewhere in considerable detail.[5,41] Briefly, the TOF mass spectra are the time histograms of ions arriving during the 2 μs which follow the onset of a pulsed extraction voltage (+ 480 V at 50 kHz) applied to the first electrode of the extraction zone (Fig. 3). The ions are detected at the end of the drift region with a channel plate which is assumed to have equal detection efficiency for all ions. The gas is introduced into the spectrometer through a needle to form an effusive jet. The pressure in the ionization region is estimated to be 10 to 100 times greater than the measured chamber pressure of 1×10^{-5} torr during the experiment.

The efficiency for extracting energetic ions from the photoionization region was found to be sensitive to the strength and duration of the extraction pulse. This is demonstrated in Fig. 3 which plots the branching ratios

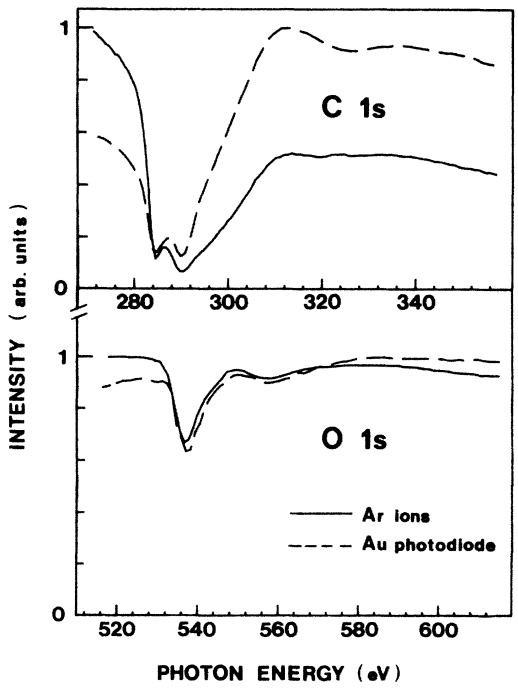

FIG. 2. Incident photon flux in the carbon and oxygen 1*s* regions as measured by a Au photodiode and by absorption-corrected Ar ion yield signals.

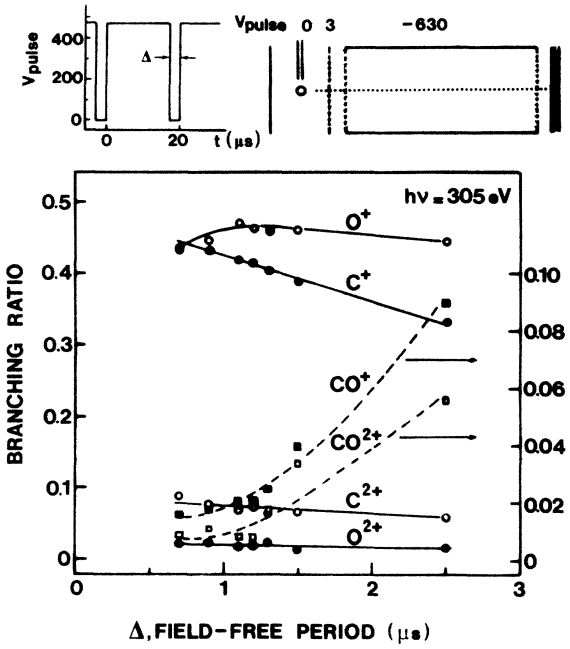

FIG. 3. (Upper) schematic of the ionization region, time-of-flight spectrometer, and the extraction pulse sequence employed. The leading edge of the pulse serves as the start signal for the time-to-amplitude converter which is stopped by an ion arriving during the high extraction voltage region of the pulse. (Lower) branching ratios for ion production at $h\nu = 305$ eV measured as a function of Δ, the off time of the extraction pulse.

at a photon energy of 305 eV for all ions as a function of Δ, the off time of the extraction pulse. The decline in the yield of the energetic atomic ions and the rapid increase in the yields of the thermal CO^+ and CO^{2+} ions which is observed with increased Δ is a result of the escape of the more energetic atomic ions from the interaction region during the absence of the extraction field. The branching ratios (BR) shown in Fig. 3 are a function of the ion kinetic energy distributions which vary slightly over the photon energies we have studied. At 305 eV the BR's appear to stabilize for off times less than 1.0 μs suggesting that representative ion collection is obtained under these conditions. Since our PIPICO measurements indicate an average kinetic energy at 305 eV that is similar to that at all other energies (see Sec. III B and Table III), we believe that there is relatively little variation of our collection efficiency over the ranges of photon energies studied. The TOF mass spectra used to determine the partial ion oscillator strengths were obtained using $\Delta = 0.7$ μs with a 480-V, 50-kHz extraction pulse. These conditions were a compromise between minimizing discrimination against energetic ions while retaining a sufficient signal for good statistics in reasonable time. The branching ratios were found to be independent of reasonable variations in the potential of the TOF drift tube (500–1200 V) and of a small potential (−5 to 10 V) applied to the entrance grid of the drift tube in order to reduce the penetration of the TOF field into the ionization region. These potentials were adjusted to optimize the mass spectral peak shapes.

III. RESULTS

A. Noncoincident measurements

1. *Total ion yield spectra*

Figure 4 presents the total ion yields measured in the C 1s and O 1s regions using continuous high-field extraction [V(source) = 750 V, V(acc) = 1500 V]. These spectra have been normalized by setting the 1s continuum intensity to 0.013 eV^{-1} at 321 eV and to 0.0077 eV^{-1} at 567 eV. These values are the calculated atomic core ionization oscillator strengths,[42] multiplied by the dissociative multiple-ionization efficiencies (η, where we define η as the number of ions produced per absorbed photon, independent of the ion charge) derived from the ion yield and PIPICO results (Sec. III B 1). The equivalence of molecular and the sum of atomic inner-shell oscillator strengths outside of the near-edge resonance region has been demonstrated previously.[43] In Fig. 4 the total ion yield spectra are compared to the corresponding C 1s and O 1s absorption spectra, as derived from dipole-limit electron energy loss spectra.[44] The resolution of each absorption spectrum has been artificially degraded by multiple three-point smooths until the full width at half maximum of the $1s \rightarrow \pi^*$ peaks was the same as in the total yield spectrum.

In both the C 1s and O 1s regions, the total ion yield is similar in shape to the true absorption spectrum but differs quantitatively because of dissociative multiple ionization ($\eta > 1$) and because of variations in η with energy.

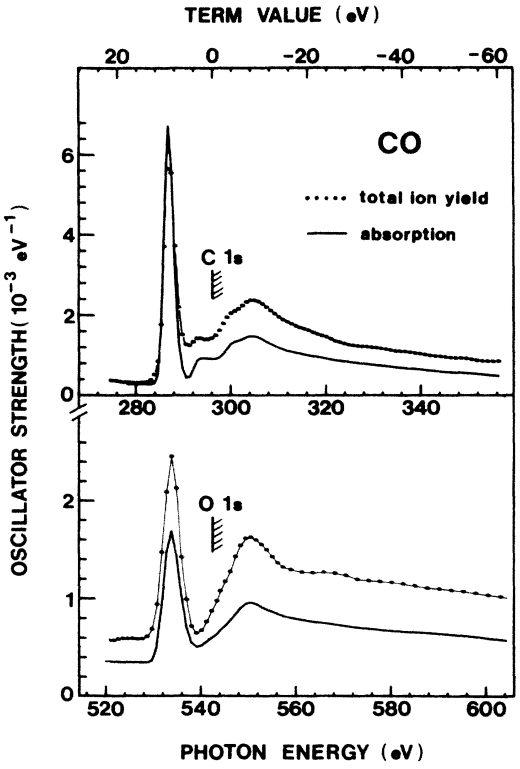

FIG. 4. Total ion yield (dots) and photoabsorption spectra (solid line) (Ref. 44) of CO in the C 1s and O 1s regions. The vertical lines followed by hatching indicate the location of the ionization thresholds, the zero point of the indicated term value scale. The absolute oscillator strengths were determined by normalization at 25 eV above the ionization potential to calculated atomic 1s values (Ref. 42). The total ion yield normalizations were additionally corrected for the dissociative multiple-ionization efficiency (Table II). The absorption spectra have been multiply three-point smoothed to give a π^* peak width similar to that in the total ion yield spectra.

Because of the resolution adjustment, Fig. 4 should be regarded as only semiquantitative. Analysis of the unmodified spectra allows a more precise comparison of the absorption and ion yield results. This provides a check on the η values, which increase from $\simeq 1.15$ at 280 eV in the valence continuum, to 1.3 at the π^* resonances, and then to 1.7 in the 1s continua, according to our results (see Sec. III B 1). The ratio of the integrated C $1s \rightarrow \pi^*$ oscillator strength (OS) to the integrated C 1s continuum between 300 and 320 eV is 0.49 in the total ion yield but 0.74 in the absorption spectrum, consistent with the variation in η(OS: 0.74/0.49 = 1.51; η: 1.70/1.27 = 1.34). The corresponding ratios of the O $1s \rightarrow \pi^*$ and O $1s \rightarrow$continuum (545–565 eV) intensities are 0.43 (ion yield) and 0.55 (absorption), again in reasonable agreement with our derived dissociative multiple-ionization efficiencies (OS: 0.55/0.42 = 1.28; η: 1.71/1.29 = 1.33). To our knowledge this is the first quantitative observation and analysis of differences between absorption and ion yield signals for inner-shell excitation and ionization of gases.

2. *Partial ion yield spectra*

Sample time-of-flight mass spectra recorded at six different photon energies are presented in Fig. 5. The vertical scale of each spectrum has been normalized to the total number of ions recorded in the same period to facilitate intensity comparisons among the six spectra. The mass resolution is somewhat lower in the spectra obtained in the O 1*s* than in the C 1*s* region because of small differences in the extraction fields. The similar magnitude of the C^+ and O^+ signals from core ionization provides further evidence for a representative collection of energetic ions under the conditions used. The $I(C^+)/I(O^+)$ ratio is 0.90±0.05 in both the C 1*s* and O 1*s* ionization continua. Following Auger decay of the 1*s* states, a final charge state of at least 2+ must exist. Since the yields of CO^{2+}, C^{2+}, and O^{2+} are all very small, symmetric dissociative double ionization producing C^+ and O^+ dominates. Thus a $I(C^+)/I(O^+)$ ratio close to 1 is expected in the 1*s* continua and should be observed, if the discrimination against high kinetic energy ions is not excessive and if the ion sampling is representative (see below). There are several processes which compete with $(C^+ + O^+)$ pair production at photon energies in the core ionization continua and which explain our observation of a $I(C^+)/I(O^+)$ ratio somewhat lower than 1.0. These include the underlying valence ionization, which produces ions of lower kinetic energy with a $I(C^+)/I(O^+)$ ratio of 0.97(4); and the triple ionization shake-off processes producing predominantly $(C^{2+} + O^+)$ with a yield of about 10% of the 1*s* continuum signal (Sec. III C). Finally there is a small discrimination of about 7% against O^+ because of the earlier arrival of the C^+ ions from $C^+ + O^+$ events.

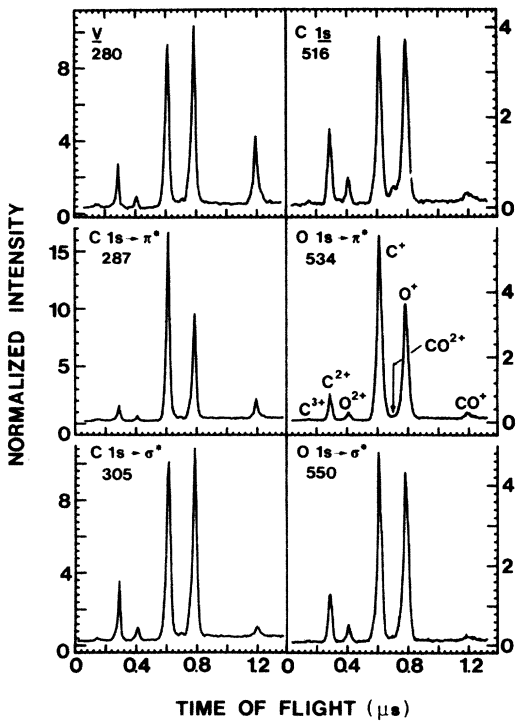

FIG. 5. Time-of-flight mass spectra recorded with the indicated photon energies (in eV) under conditions of high efficiency for fast ions [V(source)=480, V(acc)=800 V]. The intensity scales are proportional to the counts per channel divided by the total ion signal recorded in the same period.

Naively, one might expect that only C^+ would be detected from the events producing $(C^+ + O^+)$ since the lighter C^+ ion arrives before its heavier O^+ partner. Strong discrimination against O^+ would certainly occur if the overall detection efficiency of the TOF spectrometer approached 100%. However, a 50% transmission of three grids in the TOF spectrometer, and a channel plate efficiency for ion detection of about 14% (Ref. 45) combine to limit the overall efficiency of the spectrometer to about 7% (the evaluation of this figure is discussed in Sec. III B). Under these conditions the O^+ from $(C^+ + O^+)$ events will be detected (with approximately 7% probability) in the 93% of the events in which its C^+ partner is not detected. Thus we believe our spectrometer provides *representative* detection of both ions from dissociative double ionization events, with a 7% bias in favor of the lighter C^+ or C^{2+} ion. In systems with higher overall efficiencies the problem of masking of the heavier ion needs to be addressed.[46]

Time-of-flight mass spectra like those in Fig. 5 were recorded between 270 and 360 eV and between 515 and 615 eV. The areas under the ion peaks and several background regions in each of these TOF mass spectra were determined on line and saved for further processing. For each ion the relative yield was derived by subtracting background signals appropriately weighted for minor nonlinearities in the background. These relative ion yield spectra were then divided by the incident photon flux, as measured by the absorption-corrected[40] total ion yield signal of Ar (recorded separately), and corrected for the decline of the ACO stored current during the multihour acquisition of the partial ion yield spectra. An absolute oscillator strength scale was then determined by normalizing the sum of the core continuum ion signals [i.e., after subtracting underlying valence ionization signal v in the C 1*s* region and $(v + \text{C } 1s)$ signal in the O 1*s* region] to values of 0.0131 eV^{-1} at 321 eV (C 1*s*) and 0.0077 eV^{-1} at 567 eV (O 1*s*). These values are the calculated core ionization oscillator strengths for carbon and oxygen atoms[42] multiplied by η's of 1.70 at 321 eV and 1.71 at 567 eV (Sec. III B 1). The partial ion yield spectra for the C 1*s* and O 1*s* regions obtained in this manner are presented in Figs. 6 and 7, respectively.

A minor systematic error in these results is the presence of small contributions from N^+ and N_2^+ to the (weak) $m/e = 14$ (CO^{2+}) and 28 (CO^+) signals. This is indicated by the N^{2+} signal which is just barely apparent in the time-of-flight spectrum at 516 eV (Fig. 5) where the CO ionization signal is small yet the photon energy is above the nitrogen K-shell threshold. Corrections have not been made for this. In each of the mass spectra shown in Fig. 5 a weak C^{3+} signal ($m/e = 4$) is observed, with an intensity $< 1\%$ in C 1*s* and $< 0.4\%$ in O 1*s*. The spectral dependence of this signal is not presented. The C^{3+} ion yield spectrum in the O 1*s* region was similar to that found for CO^{2+} (Fig. 7), i.e., the C^{3+} signal does not

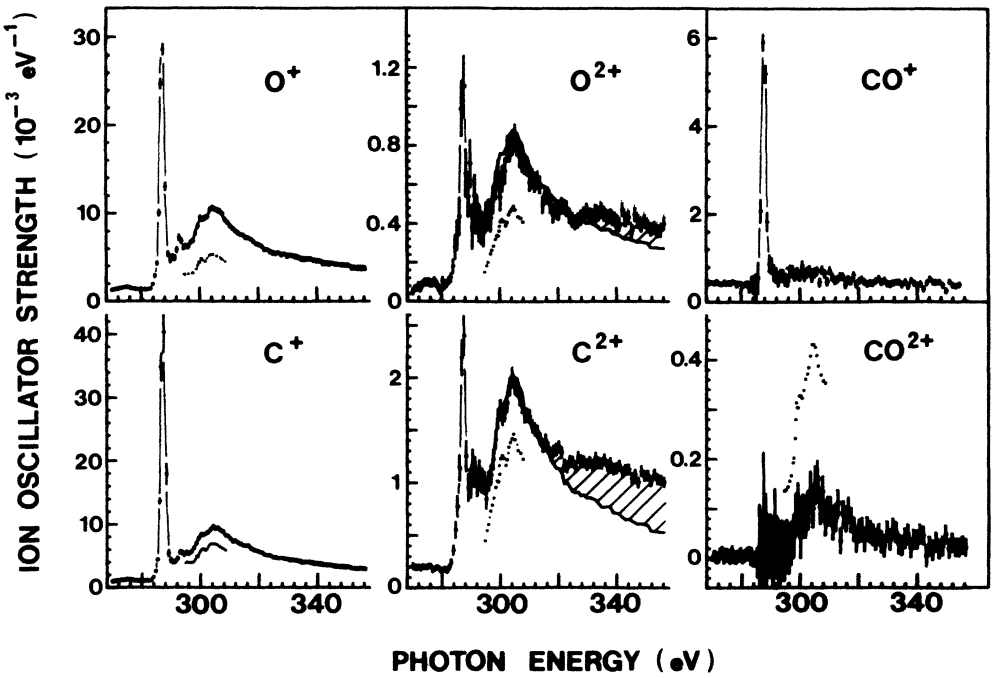

FIG. 6. Partial ion yield oscillator strengths from C 1s photoionization of CO. The absolute scales were established by normalization at 321 eV to calculated atomic cross sections for C 1s ionization with a correction for dissociative multiple ionization derived from the PIPICO signal. Dots are the $(e,e+\text{ion})$ results of Kay *et al.* (Ref. 17). Solid lines are the total ion yield spectrum scaled to match each ion yield spectrum between 296 and 310 eV. The hatching highlights the difference between the shapes of the absorption and partial yield curves which are assigned to multielectron processes (see text).

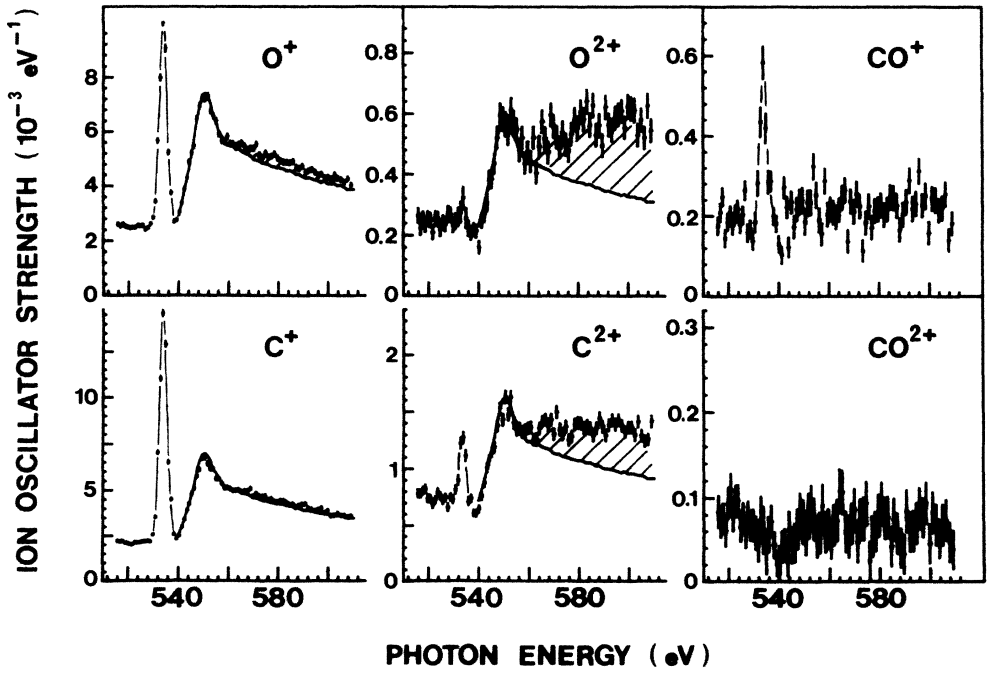

FIG. 7. Partial ion yield oscillator strengths from O 1s photoionization of CO. The absolute scales were established by normalization at 565 eV to calculated atomic cross sections with a correction for dissociative multiple ionization derived from the PIPICO signal. Solid lines are the total ion yield spectrum scaled to match each ion yield spectrum between 542 and 554 eV. Hatching as explained in Fig. 6.

resonate at the O $1s \rightarrow \pi^*$ energy.

There are considerable differences between the present results and most previous measurements of the ionic fragmentation following C 1*s* excitation in gaseous CO.[1,2,17,18,33] In particular, the parent ion yield is smaller and the C^+ and O^+ yields are larger than in almost all previous work. These differences are consistent with kinetic energy discrimination effects. In experiments using quadrupole mass filters, CO^+ yields up to 70% in the C 1*s* continuum have been reported.[1,2] We believe such large values result from the escape of energetic atomic ions from the quadrupole filter.

In general our results are in good agreement with the most recent TOF measurements of Eberhardt *et al.*,[18,23] although our yields of the thermal ions are still slightly lower. Our results at 550 eV, above the O 1*s* edge, also compare well with those obtained at 552 eV by Sato *et al.*[35] and at 930 eV by Carlson and Krause,[16] taking into account the gradual increase of the C^{2+} and O^{2+} yields at higher energy. We note that the mass spectrometer of Carlson and Krause was designed to avoid discrimination against high kinetic energy ions. Simulations of our ion extraction fields indicate that all ions produced with less than 5 eV kinetic energy are collected and that the collection efficiency declines to 50% only for ions with kinetic energies greater than 12 eV. Although our TOF spectra are still slightly distorted by kinetic energy discrimination, we believe that our results are a better representation of the true ion yields than those given previously. It is clear that great care is needed when studying ion yields from core excitation since almost invariably these will involve high ion kinetic energies. For example, different levels of kinetic energy discrimination may explain the substantial differences that exist in the two published measurements of the ion yields from core excitation of acetone.[1,5]

The partial ion oscillator strength spectra in the C 1*s* region (Fig. 6) are compared to those derived from the $(e,e+\text{ion})$ measurements.[17] Since Kay *et al.*[17] present only the sum of $C^+ + O^+$ and $C^{2+} + O^{2+}$ signals we have used their 305-eV branching ratios to derive the individual $(e,e+\text{ion})$ atomic ion curves shown in Fig. 6. In general the magnitudes and shapes are similar (within statistical uncertainties) although, *relatively,* the oscillator strength for atomic ions are higher and those for the molecular ions (both CO^+ and CO^{2+}) somewhat lower in the present work, presumably reflecting less kinetic energy discrimination in our ion extraction procedures. Our *absolute* oscillator strengths for the dominant atomic fragment ions are all approximately 70% larger than those reported earlier.[17] This difference arises because we believe that we have representative detection of all ions and thus have used an absorption scale corrected for a dissociative multiple-ionization efficiency of 1.7 (in the continuum) whereas Kay *et al.*[17] have assumed that the sum of their ion signals would be identical to the absorption. If the $(e,e+\text{ion})$ spectrometer detects only one of the two ions produced in dissociative double ionization, as they state, then this assumption is reasonable. Their $I(C^+)/I(O^+)$ ratio, which was constant over the 296–310-eV energy range studied by $(e,e+\text{ion})$,[17] is 1.3, almost 50% larger than the value of 0.9 we find for the C 1*s* continuum. This is consistent with a relatively strong masking of the O^+ by the C^+ signal under the $(e,e+\text{ion})$ extraction conditions. However, the O^+ yield is still much larger than can be explained by underlying valence ionization (the only channel producing O^+ without a lighter C^+ or C^{2+} partner), and thus 100% collection efficiency (or, equivalently, 100% masking) was not achieved.

3. *Branching ratios*

The branching ratio spectrum for each ion was derived from its ion yield spectrum by dividing by the sum of all partial ion yield spectra. These results are plotted in Figs. 8 (C 1*s*) and 9 (O 1*s*). Table I presents the branching ratios at selected energies, derived from the high statistics spectra of Fig. 5. There are minor differences between the data of Table I and that reported in Figs. 8 and 9, in part because of the better statistical precision of the TOF spectra recorded at selected photon energies and in part because of small differences in the experimental conditions. In Table I our results are compared with the results of earlier gas phase measurements in the C 1*s* region,[2,17,18] O 1*s* region,[34,35] and at 930 eV.[16]

In contrast to the essentially constant ion branching ratios in the core ionization continua, there are large increases in the C^+ yield, and significant decreases in the C^{2+} and O^{2+} yields at the π^* resonances (Figs. 5, 8, and 9). The $I(C^+)/I(O^+)$ ratio for the C $\underline{1s}\pi^*$ state is 1.68(6)

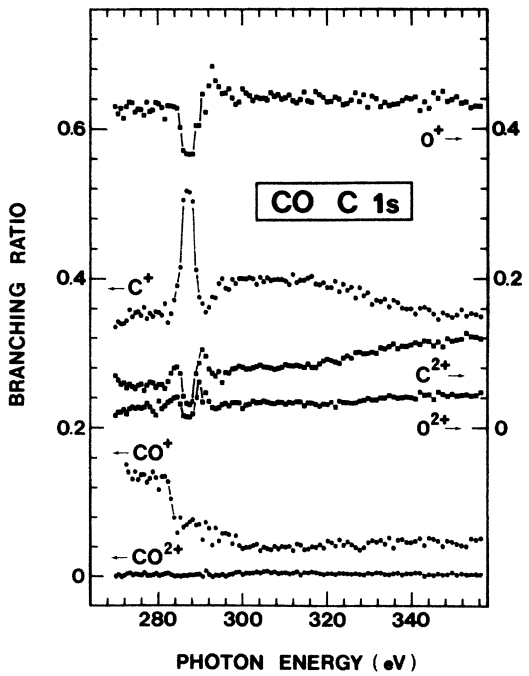

FIG. 8. Branching ratios for ion production in the C 1*s* region. Note that the right-hand scale is to be used for the displaced O^+, C^{2+}, and O^{2+} curves.

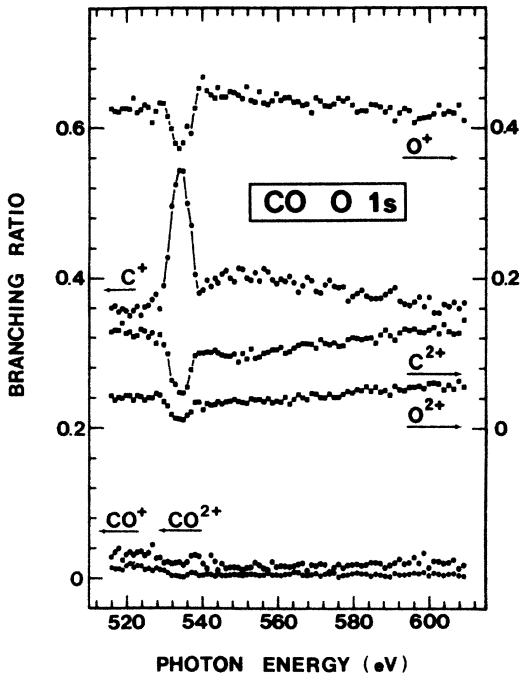

FIG. 9. Branching ratios for ion production in the O 1s region. Note that the right-hand scale is to be used for the displaced O^+, C^{2+}, and O^{2+} curves.

while that for the O $\underline{1s}\pi^*$ state is 1.49(4). These rather similar $I(C^+)/I(O^+)$ ratios indicate that the *site* of the core hole in CO has relatively little influence on the final ion distribution, in contrast to previous indications of site-selective fragmentation and ionization in N_2O,[47] acetone,[1] and CF_3CH_3 (Ref. 3) (see Sec. IV D for discussion). We do note, however, that the O^{2+} yield from the O $1s\rightarrow\pi^*$ and the C $1s\rightarrow\pi^*$ transitions differ qualitatively in that the O^{2+} yield from the O $1s\rightarrow\pi^*$ transition is essentially zero (Fig. 7).

All of the atomic partial ion yield spectra appear to have the same shape in the $1s\rightarrow\sigma^*$ regions between 298 and 315 eV and between 544 and 558 eV. This suggests that the electronic decay of the $1s\rightarrow\sigma^*$ resonances and the surrounding nonresonance continuum is the same. A simplified model of the resonance is as a temporary $\underline{1s}\sigma^*$ state superimposed on the normal, direct 1s ionization continuum. From this viewpoint one might expect the σ^* state to be coupled uniquely to the 1s continuum following the usual one-electron picture of shape resonances.[48] The intensity of the subsequent Auger decay process and thus the ion yields are also expected to be enhanced at the resonance energy. In this picture one assumes that the primary photoelectron ejection, the Auger decay, and the fragmentation of the doubly valence ionized states are sequential events. If the resonance is effective in exciting vibrational motion of the $\underline{1s}$ ionic state or if fragmentation occurs before the Auger decay, the partial ion yield could be quite different on and off resonance. The absence of selective fragmentation processes at the C $1s\rightarrow\sigma^*$ resonances suggests these conditions are not met, as has been noted previously for the much stronger and narrower t_{2g} and e_g resonances in the S 2p spectrum of SF_6 (Ref. 46) and also found for prominent σ^* resonances in the C 1s and N 1s spectra of CH_3CN.[8]

There is a significant rise in the C^{2+} and O^{2+} yields at energies above 320 eV and above 560 eV. This is most clearly seen in Figs. 6 and 7, where the continuum shapes of the C^{2+} and O^{2+} and the total ion spectra are compared and the difference is shaded. The differences above 320 and 560 eV occur because of the opening of shake-up and/or shake-off channels. These have increased C^{2+} and O^{2+} yields as compared to the main C $\underline{1s}$ and O $\underline{1s}$ channels. The clear observation of the shake continua in these partial ion yield spectra supports the conclusion that rather rapid rises in the shake processes can occur above threshold and thus a rapid convergence from the adiabatic to the sudden regime[49,50] can take place, at least in certain cases. In principle, the cross sections for multielectron processes can be derived by comparing photoelectron and Auger cross sections with absorption spectra. Such a comparison has been reported recently for CO.[51] Unfortunately, the measurements were only made up to 315 eV in the C 1s region. However, in the O 1s region, where the measurements extended from the O 1s threshold (542.0 eV) to 635 eV, the photoelectron main line cross sections were significantly below the photoabsorption curve[52] above 560 eV, consistent with our observations.

Reimer *et al.*[53] have recently measured the photoemission cross sections between 300 and 400 eV for the production of two C 1s shake-up satellites in CO. They find $\simeq 10\%$ satellite contributions in this region. The partial cross section for the 308-eV shake-up line is similar to that of the C $\underline{1s}$ main line but displaced by the additional shake energy. Its maximum at 320 eV cannot be matched easily to any of the partial ion yield features. The higher-energy shake up at 315 eV has a cross section which increases slowly but continually between 340 and 400 eV. Again this feature is not easily correlated with the hatched regions in Fig. 6. The shake-off continuum (threshold $\cong 318$ eV) has an appreciable magnitude in the 390-eV photoelectron spectrum presented by Reimer *et al.*[53] Unfortunately its partial cross section was not measured, but we expect it to be similar to the hatched region in Fig. 7. The increased C^{2+} and O^{2+} production that we observe above 320 eV in the C 1s region is accompanied by a small drop in the C^+ yield (relative to the total continuum shape). This is as expected since the $(C^+ + O^{2+})$ channel is very weak and thus there is no compensation, as appears to occur in the O^+ signal, where the reduced O^+ branching ratio from the relative decrease in the $(C^+ + O^+)$ yield is replaced by O^+ from $(C^{2+} + O^+)$, produced preferentially in the shake-off continua. In the O 1s region the O^+ yield above 560 eV exceeds that of the scaled total ion yield, again evidence for large amounts of decay to $(C^{2+} + O^+)$ in the shake-off continuum. The multielectron processes giving rise to the enhanced C^{2+} and O^{2+} yields above 320 and 560 eV are discussed further in Sec. IV C.

TABLE I. Ion-branching ratios following soft x-ray photoionization of CO.

		v		C $1s\pi^*$			C $1s$		
	140 eV	280 eV		287.5 eV			305 eV		
Ion	a	b	c1	b	c1	a	b	c1	a
CO^+	0.47	0.153(6)	0.46	0.068(5)	0.17	0.085	0.030(4)	0.05	0.04
O^+	0.240	0.377(7)	0.26	0.324(7)	0.24	0.312	0.419(7)	0.35	0.40
C^+	0.117	0.366(7)	0.22	0.546(8)	0.51	0.53	0.424(7)	0.45	0.31
CO^{2+}	0.028	0.013(2)	0.02	0.006(2)	0.02	0.025	0.011(2)	0.03	0.05
O^{2+}	0.017	0.021(2)	0.01	0.014(2)	0.02	0.013	0.027(2)	0.03	0.05
C^{2+}	0.063	0.070(3)	0.02	0.043(3)	0.05	0.049	0.088(3)	0.08	0.16
C^{3+}		0.001(4)		0.012(3)			0.013(4)		
$O^+ + C^+$	0.36	0.74(1)	0.48	0.87(1)	0.75	0.84	0.84(1)	0.80	0.71
$O^{2+} + C^{2+}$	0.08	0.091(5)	0.03	0.057(4)	0.07	0.06	0.115(5)	0.11	0.21
C^+/O^+	0.49	0.97(4)	0.985	1.68(6)	2.1	1.69	1.01(3)	1.3	0.75
$I(C^{2+})/I(O^{2+})$	3.7	3.3(5)	2	3.1(7)	2.5	3.8	3.3(4)	2.7	3.4

	C $1s$	O $1s\pi^*$			O $1s$		
	516	534			550		930
Ion	b	b	c2	b	c2	d	e
CO^+	0.021(6)	0.013(3)	0.04(3)	0.009(3)	0.13(4)	0.06	0.05(2)
O^+	0.402(13)	0.369(6)	0.28(5)	0.435(8)	0.37(19)	0.38	0.40(2)
C^+	0.368(11)	0.551(7)	0.50(9)	0.419(7)	0.32(17)	0.38	0.34(2)
CO^{2+}	0.033(4)[f]	0.009(2)	0.05(3)	0.014(2)	0.02(7)	0.02	0.008(2)
O^{2+}	0.044(5)	0.012(2)	0.06(3)	0.031(3)	0.06(8)	0.06	0.044(8)
C^{2+}	0.128(7)	0.046(2)	0.08(3)	0.091(4)	0.10(9)	0.12	0.14(3)
C^{3+}	0.004(3)	0.000(1)		0.001(2)			0.008(4)
$O^+ + C^+$	0.77(2)	0.92(1)	0.78	0.85(1)	0.69	0.76	0.74
$O^{2+} + C^{2+}$	0.172(12)	0.058(4)	0.14	0.122(7)	0.16	0.18	0.184
C^+/O^+	0.92(6)	1.49(4)	1.8	0.96(3)	0.86	1.00	0.85
$I(C^{2+})/I(O^{2+})$	2.9(5)	3.8(8)	1.3	2.9(4)	1.7	2.0	3.2

[a]Derived from peak integration of the time-of-flight mass spectra plotted in Refs. 18 and 23.
[b]This work.
[c]From published (Ref. 17) (c1) and unpublished (e,e + ion) spectroscopy (Ref. 34) (c2).
[d]Unpublished TOF photoionization results (Ref. 35).
[e]Custom photoionization mass spectrometer, optimized for the quantitative collection of energetic ions (Ref. 16).
[f]Significant contributions from N_2^{2+} are expected to contribute to the CO^{2+} yield at 516 eV.

B. Photoion-photoion coincidences

1. Strong-field PIPICO

The relative strengths of dissociative multiple-ionization processes were measured at six selected photon energies by the PIPICO method. The PIPICO spectra were recorded without an Al filter in the C 1s region and with an Al filter in the O 1s region in order to reduce the stray light. Two different ion extraction fields were used for these measurements. Figure 10 presents the PIPICO spectrum obtained with a high extraction field and $h\nu = 305$ eV, at the C $1s\sigma^*$ resonance. Even under these high-field conditions [V(source)$=750$, V(acc)$=1500$ V] there is some discrimination against high kinetic energy ions as indicated by the double peaked line shapes. Three possible signals from dissociative multiple ionization of CO can contribute to the PIPICO spectra: $(C^+ + O^+)$, $(C^{2+} + O^+)$, and $(C^+ + O^{2+})$. Of these, the $(C^+ + O^+)$ dominates, the $(C^{2+} + O^+)$ is weak but well resolved, while evidence for the $(C^+ + O^{2+})$ signal exists in the 305 and 550-eV spectra, in the form of a shoulder on the high ΔTOF side of the intense $(C^+ + O^+)$ signal.

The vertical lines in Fig. 10 indicate for each pair production process the peak positions calculated from the average kinetic energy released determined in the weak-field PIPICO (Sec. III B 2). The average kinetic energy released in the $C^+ + O^{2+}$ process was assumed to be identical to that for the $C^{2+} + O^+$ process. The good match observed between the calculated $C^{2+} + O^+$ peak position and the shoulder on the $(C^+ + O^+)$ peak at 0.21-μs time-of-flight difference supports our assignment of this feature to $(C^+ + O^{2+})$. An estimated upper bound to the $(C^+ + O^{2+})$ yield of 2% of the total ion-pair production

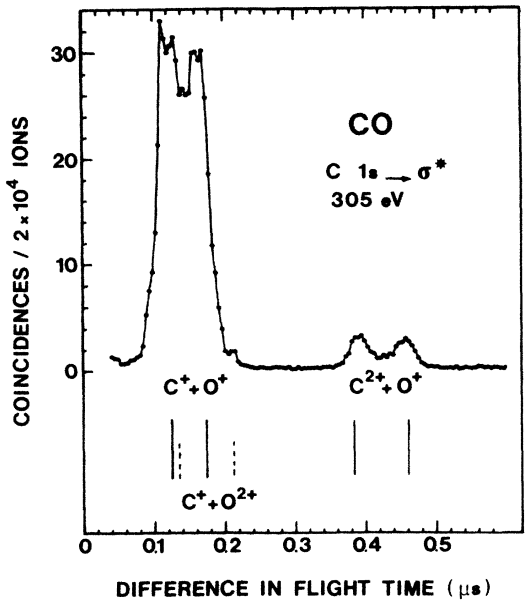

FIG. 10. Photoion-photoion coincidence (PIPICO) spectrum of CO recorded with strong extraction field at $h\nu = 305$ eV. The lines indicate the peak positions predicted for the experimental conditions [V(source) = 750, V(acc) = 1500 V] and a total kinetic energy equal to 14.8 eV for $(C^+ + O^+)$ and 25 eV for $(C^{2+} + O^+)$ and $(C^+ + O^{2+})$.

was derived from integration of the highest-energy portion of the $(C^+ + O^+)$ PIPICO peak ($h\nu = 305$ eV). The weakness of the $(C^+ + O^{2+})$ relative to the $(C^{2+} + O^+)$ channel is consistent with the individual ion yields since the C^{2+} signal (measured without coincidence) is stronger than the O^{2+} signal at all energies (see Figs. 6 and 7). Kay *et al.*[17] have also argued that the $(C^+ + O^{2+})$ channel is weak or nonexistent, based on their estimates of the individual C^{2+} and O^{2+} kinetic energies in the C 1*s* region.

In order to relate quantitatively the PIPICO intensities at high extraction fields with the noncoincident ion yields, a correction for the detection efficiency of the spectrometer is required. The overall detection efficiency is composed of a channel plate contribution of $\simeq 14\%$ combined with a probability for transmission through the TOF spectrometer of $\simeq 50\%$. The ion-pair production, N(pairs) relative to all ionization events, N(total) is related to the experimental results through[41]

$$\frac{N(\text{pairs})}{N(\text{total})} = \frac{1}{(N_{\text{singles}}/\Sigma N_{\text{pairs}})f - 1} ,$$

where N_{singles} is the total number of ions detected during the same period that ΣN_{pairs} PIPICO events are detected; N(pairs)/N(total) represents the fraction of all ionization events that result in two ions and f is the overall detection efficiency of the spectrometer. We note that the underlying valence ionization continuum contributes 20% of the signal at 305 eV. If we assume that 84% of the C 1*s* ionization results in pair production (the maximum value that avoids negative reaction yields—see Sec. III B 3), then we derive a detection efficiency of 7.1% from comparison of the PIPICO yields at 280 and 305 eV. With this detection efficiency, the relative proportions of ion-pair production and the dissociative multiple-ionization efficiency at each photon energy are as given in Table II.

2. *Weak-field PIPICO: Ion kinetic energy released distributions*

The PIPICO spectrum obtained at 305 eV with a weak extraction field [V(source) = 60, V(acc) = 95 V] is shown in Fig. 11 along with a simulation of this signal based on the experimental conditions and the $(C^+ + O^+)$ and $(C^{2+} + O^+)$ kinetic energy released distributions (KERD's) at 305 eV (Table III). In the weak-field case

TABLE II. Dissociative multiple-ionization efficiencies (η) and PIPICO ion-pair yields.

Photon energy (eV)	η[a]	Pair partial yields (C^+,O^+)	(C^{2+},O^+)	N(pairs)/N(total)	Al filter
280	1.15	0.13	0.02	0.15	no
287	1.27	0.25	0.02	0.27	no
305	(1.70)	0.65	0.05	(0.70)[b]	no
516	1.59[c]	0.50	0.09	0.59	yes
534	1.29	0.27	0.02	0.29	yes
550	1.71	0.63	0.08	0.71	yes

[a] η is defined as the number of ions produced per photon absorbed, independent of the ion charge.
[b] An overall detection efficiency of 7.1% was derived from the relative PIPICO yields at 280 and 305 eV, based on a 20% valence contribution at 305 eV [measured from the total ion yield spectrum (Fig. 4)] and assuming 84% ion pair production following C 1*s* ionization at 305 eV (thus the 0.70 pair yield at 305 eV is composed of 0.84*0.80 = 0.67 from C 1*s* ionization and 0.15*0.20 = 0.03 from valence ionization). The other yields of dissociative multiple ionization were then derived from the measured N(singles)/ΣN(pairs) ratios, using this detection efficiency and the equation given in the text.
[c] The decrease in η (516 eV) relative to η (305 eV) reflects a relatively greater contribution of the underlying valence continuum $\underline{v}$ at 516 eV (where the C 1*s* ionization cross section has decayed considerably) than at 305 eV (the maximum of the σ^* resonance). A proportion of 35% ($\underline{v}$) and 65% (C $\underline{1s}$) at 516 eV with $\eta(\underline{v}) = 1.15$ and η (C $\underline{1s}$) = 1.84 gives consistent results at 305 and 516 eV.

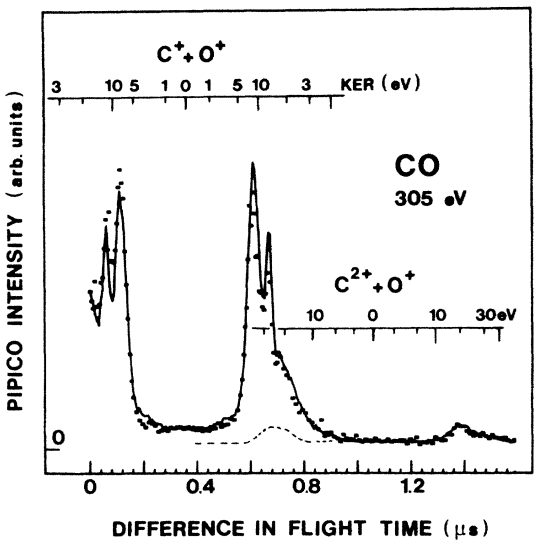

FIG. 11. Photoion-photoion coincidence (PIPICO) spectrum of CO recorded with weak extraction field at $h\nu = 305$ eV. The points are the experimental data while the solid line is the result of a Monte Carlo simulation based on the experimental conditions [V(source) = 60, V(acc) = 95 V] and the ion kinetic energies for the $(C^+ + O^+)$ and $(C^{2+} + O^+)$ pairs summarized in Table III. The dashed line indicates the $(C^{2+} + O^+)$ contribution from events in which the C^{2+} ion initially moved away from the TOF spectrometer.

discrimination against high kinetic energy ions makes the PIPICO peak shapes very sensitive to the kinetic energy released distributions.[41]

The total kinetic energies released to $(C^+ + O^+)$ and $(C^{2+} + O^+)$ ion pairs produced in dissociative double and triple ionization were estimated from the peak shapes in the weak-field PIPICO spectra by a simulation technique in which the PIPICO signal was calculated by a Monte Carlo method for the experimental geometry, applied fields, and assumed multicomponent KERD's. The average kinetic energy released (KER), the energy spread full width at half maximum (FWHM), and the relative population of each of the components was then varied until a good fit to the observed PIPICO peak shape was obtained.

The dominant $(C^+ + O^+)$ coincidence signals at all six energies are shown in Fig. 12, in comparison with the calculated peak shapes. The component of the $(C^{2+} + O^+)$ signal which underlies the $(C^+ + O^+)$ signal (dashed line in Fig. 11) has not been accounted for in the fits shown in Fig. 12. Based on a simultaneous fit to both the $(C^+ + O^+)$ and $(C^{2+} + O^+)$ signals at 550 eV, the major effect of this $(C^{2+} + O^+)$ signal is to reduce the component around 17 eV released kinetic energy in the $(C^+ + O^+)$ KERD's at 305, 516, and 550 eV. Simulations of the $(C^{2+} + O^+)$ signals at 305 and 550 eV yield an average kinetic energy released of 25 eV with a two-component distribution of (20 eV, 10 eV, 1.0) and (30 eV, 20 eV, 1.0) average energy, width, and weights, respectively. The $(C^{2+} + O^+)$ signal is negligible at the other

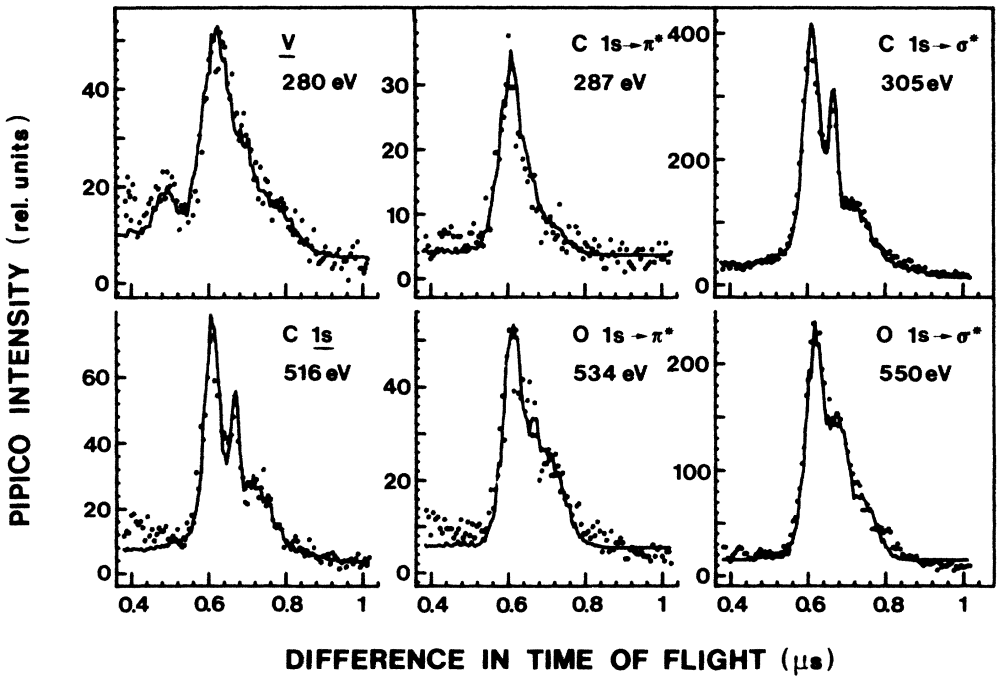

FIG. 12. The weak-field PIPICO spectra in the region of the $(C^+ + O^+)$ peak. The dots are the experimental data while the solid lines are the results of Monte Carlo simulations based on the $(C^+ + O^+)$ ion kinetic energy release distributions summarized in Table III.

TABLE III. $(C^+ + O^+)$ ion kinetic energy distributions from PIPICO.

				Valence continuum					
		110 eV[a]			280 eV				
	E	FWHM	weight	E	FWHM	weight			
	1.8	1.5	0.01	2.7	1.8	0.06			
	3.8	3	0.12						
	7.7	2.1	0.07	9.0	4.8	0.8			
	10.9	5.7	0.48						
	15.7	3.3	0.05	14	6.0	0.4			
	21.7	11.5	0.34	20	18.0	1.2			
E(avg)		13.4			15.0				
				π^* resonances					
		287 eV			534 eV				
	8.5	4.0	1.0	8.7	3.5	1.0			
	12.5	3.0	0.2	12.5	3.0	0.35			
	16.0	10.0	0.5	16.0	8.0	1.0			
E(avg)		11.2			12.4				
				Inner-shell continua					
		305 eV[b]			516 eV			550 eV[b]	
	4.0	5.0	0.08	4.0	5.0	0.08	4.0	5.0	0.06
	8.6	3.0	1.0	8.4	2.8	1.0	9.2	3.5	1.0
	12.5	2.0	0.48	12.5	2.0	0.45	13.5	4.5	0.8
	17.0	12.0	1.3	17.0	12.0	1.6	17.0	12.0	1.6
	28	20.0	0.4	28.0	20.0	0.4	28.0	20.0	0.4
E(avg)		14.8[c]			14.9			15.0	

[a]Reference 57.

[b]When both the $(C^+ + O^+)$ and the $(C^{2+} + O^+)$ signals were simulated the fourth contribution was modified to E(avg) = 18.0, FWHM = 12.0, and weight = 0.4. All other components were required as in Table III to provide the quality of fit shown in Fig. 10. Two components with E(avg), FWHM, weight of 20 eV, 10 eV, 1 and 30 eV, 20 eV, 1, respectively, were required to simulate the $(C^{2+} + O^+)$ signal.

[c]Kay *et al.* (Ref. 17) report average kinetic energies at 305 eV of 6±2 eV for O^+, 8±2 eV for C^+, 8±2 eV for C^{2+}, and 16±8 eV for O^{2+}. Thus they predict 14±4 eV and 24±10 eV for the average kinetic energy release in $(C^+ + O^+)$ and $(C^{2+} + O^+)$ processes. These values are in reasonable agreement with the present results.

energies (see Table II). The ion kinetic energy distributions and the average KER derived from these simulations are presented in Table III.

Ion KERD's of the $(C^+ + O^+)$ channel formed by electron impact have already been reported. Brehm and de Frènes[54] using 150-eV electrons found an asymmetric distribution of $(C^+ + O^+)$ energies, ranging from 3 to 25 eV with a mean around 8 eV, while a careful study of the kinetic energy released during the decay of metastable CO^{2+} to $(C^+ + O^+)$ gave an average of 5.6(1) eV with 80-eV impact[55] and 5.3(1) eV with 70-eV impact.[56] These values are significantly lower than ours and cannot easily be compared given the different formation mechanisms. However, it appears that soft x rays form more efficiently higher-energy dissociative CO^{2+} states, which produce higher-energy atomic fragments. Lower-energy photons will also populate more efficiently the lower-lying CO^{2+} states, as shown by the KERD at 110 eV photon impact[57] (see Table III). Fluorescence produced in the decay of excited CO^{2+} states to the metastable CO^{2+} ground state has been identified recently.[58]

The average energies of our KERD's are also comparable to the sums of the individual ion kinetic energies derived from $(e,e + \text{ion})$,[17] 930-eV PIMS,[16] or from analysis of the Auger-ion coincidence peak shapes.[23] We note that the sum of the C^+ and O^+ kinetic energies is not constant at all Auger energies in the Auger-ion coincidence measurements, but rather increases as successively higher-energy dissociative CO^{2+} states are accessed (see Sec. IV A and Fig. 13). There is a large jump from 16 to 32 eV average kinetic energy release on going from 56 to 72 eV binding energy in the C 1s Auger.[23] [The Auger kinetic energy (E_k) can be converted to a binding energy (E_b) by substracting it from the core ionization energy (E_0): $E_b = E_0 - E_k$.] These higher-energy states may correspond to CO^{3+} and thus to copious $(C^{2+} + O^+)$ production, which will increase the average O^+ energy.

In the case of the $(C^{2+} + O^+)$ process, our average kinetic energy of 25 eV derived from both the 305-eV and 550-eV PIPICO spectra is in agreement with that estimated from simple coulomb repulsion considerations ($2e^2/R_e \approx 25$ eV), as found by Kay *et al.*[17] for the sum of

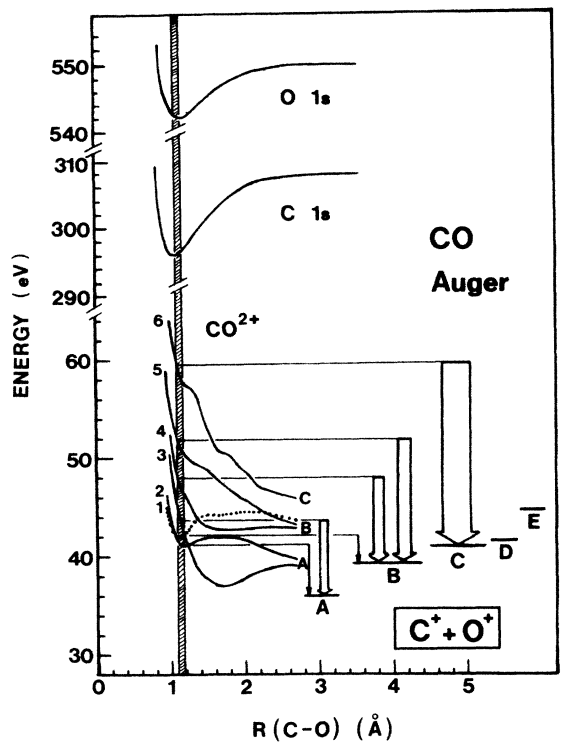

FIG. 13. Schematic of Auger decay leading to $(C^+ + O^+)$. The 1s potential curves are taken from the calculations of Correia *et al.* (Ref. 9), while those for six representative dissociative CO^{2+} states [$1 = {}^1\Sigma^+(1)$, $2 = {}^3\Pi$, $3 = {}^3\Sigma^-$, $4 = {}^1\Delta$, $5 = {}^1\Sigma^-$, $6 = {}^1\Sigma^+(2)$] are taken from the results of Wetmore *et al.* (Ref. 19). The symmetries and energies of the C^+ and O^+ limits (A–E) are listed in footnote b of Table V. The widths of the bars indicating the ion kinetic energy release are proportional to the contributions of similar ion KER observed in our C 1s and O 1s PIPICO measurements. A total of 32 CO^{2+} states leading to the lowest four $C^+ + O^+$ limits are calculated by Wetmore *et al.* Many more exist leading to $C^+ + O^+$ states only a few eV higher. Thus this figure is intended to depict the general mechanism for producing high kinetic energy $(C^+ + O^+)$ and is not intended as an exact or complete description.

their estimated C^{2+} and O^+ ion kinetic energies. It also agrees with the sum of the C^{2+} (24 eV) and O^+ (8 eV) average kinetic energies determined with 930-eV photoionization,[16] and with the average energies derived from the O^+ and C^{2+} signals measured in coincidence with Auger electrons corresponding to the production of high binding-energy states.[23]

In the PIPICO spectra recorded with a strong extraction field the peaks are less double peaked at the π^* resonances than at other energies, indicating that fewer high kinetic energy ions are produced in the autoionization of the $1s\pi^*$ state than in the continuum. This difference is observed more clearly in the weak-field PIPICO spectra (Fig. 12). The $(C^+ + O^+)$ peak has a smaller asymmetry and the average of the KERD is about 3 eV smaller at 287 and 534 eV than at the other energies (see Table III). There are also differences in the $(C^+ + O^+)$ peak shapes between 305 and 550 eV, the σ^* resonances in the C 1s and O 1s continua (Fig. 12). The biggest change here is an increase from the C 1s to the O $1s\sigma^*$ resonance in the spread of the component of the ion kinetic energy distribution around 13 eV. Although the average KER is fairly similar at all energies above 280 eV, the variation in the PIPICO peak shapes shows that there are variations in the coupling of the different core-excited states to individual dissociative CO^{2+} states. The combination of selective core excitation by tuned photoionization and Auger-ion coincidence will allow a more precise investigation of these different decays.

C. Relative contributions of the ionization reactions

Ions can be produced from photoionization of CO according to the following reactions:

Process	Ionization
	single
$h\nu + CO \rightarrow CO^+$	(a)
$h\nu + CO \rightarrow C^+ + O$	(b)
$h\nu + CO \rightarrow C + O^+$	(c)
	double
$h\nu + CO \rightarrow CO^{2+}$	(d)
$h\nu + CO \rightarrow C^{2+} + O$	(e)
$h\nu + CO \rightarrow C + O^{2+}$	(f)
$h\nu + CO \rightarrow C^+ + O^+$	(g)
	triple
$h\nu + CO \rightarrow CO^{3+}$	(h)
$h\nu + CO \rightarrow C^{3+} + O$	(i)
$h\nu + CO \rightarrow C + O^{3+}$	(j)
$h\nu + CO \rightarrow C^{2+} + O^+$	(k)
$h\nu + CO \rightarrow C^+ + O^{2+}$	(l)

Since each atomic ion can be produced by more than one process there is not a simple 1:1 relationship between the relative contributions of the above ionization reactions and the observed ion-branching ratios. Processes (g), (k), and (l) produce more than a single ion and thus are responsible for the greater than unit dissociative multiple-ionization efficiencies. Based on the negligible CO^{3+}, C^{3+}, O^{3+}, and $(C^+ + O^{2+})$ yields (Figs. 5 and 10), we have assumed $h = i = j = l = 0$. We have combined our quantitative ion yields (Table I) with the η values derived from the PIPICO measurements (Table II) in order to derive the relative contributions of the above reactions in the valence continuum, at the C 1s ad O $1s\pi^*$ resonances and at the σ^* resonances in the 1s ionization continua. Our results are summarized in Table IV. The overlap of electronic states has been accounted for in the derivation of the values listed in Table IV. For example, the PIPICO and individual ion signals at 550 eV have been divided into contributions of 65% O 1s, 28% C 1s, and 7% v, based on extrapolations of the valence and C 1s continua in the total ion yield spectrum and on the reaction yields derived at lower energies. The values reported in Table IV are in good agreement with those derived independently from branching ratios determined

TABLE IV. Relative importance of CO ionization reactions following high-energy photoabsorption.

	Relative yield[a]				
	υ	C $1s\pi^*$	O $1s\pi^*$	C $1s$	O $1s$
Reaction products	280	287	534[b]	305/516[c]	534[d]
(a) CO^+	0.18	0.09	0.02	0.00	0.01
(b) $C^+ + O$	0.29	0.44	0.53	0.03	0.09[e]
(c) $C + O^+$	0.28	0.12	0.22	0.00	0.02
(d) CO^{2+}	0.02	0.01	0.01	0.03	0.02
(e) $C^{2+} + O$	0.06	0.04	0.02	0.11	0.07
(f) $C + O^{2+}$	0.02	0.02	0.00	0.07	0.05
(g) $C^+ + O^+$	0.13	0.25	0.19	0.69	0.66
(k) $C^{2+} + O^+$	0.02	0.02	0.01	0.08	0.09

[a]Derivation (assuming $h=i=j=l=0$; R represent the branching ratios of Table I): $a=\eta R(CO^+)$, $b=\eta R(C^+)-g$, $c=\eta R(O^+)-(g+k)$, $d=\eta R(CO^{2+})$, $\eta=1+g+k$, $e=\eta R(C^{2+})-k$, $f=\eta R(O^{2+})$, $g=N_p/N_T(C^+ + O^+)$, and $k=N_p/N_T(C^{2+} + O^+)$.

[b]The values derived from the above equations have been corrected for underlying 4% (υ) and 16% (C $1s$) contributions (estimated from the backgrounds in the total yield spectrum), using the (υ) and (C $1s$) values given in this table and $\eta(C\ 1s)=1.84$.

[c]The values quoted are the average of the relative yields derived from the 305- and 516-eV data. The values listed include corrections for an underlying 20% (υ) contribution using $\eta(O\ 1s\pi^*)=1.19$.

[d]These values include a correction for an underlying 28% (C $1s$) and 7% (υ) (based on the total yield spectrum), using $\eta(O\ 1s)=1.71$.

[e]In principle, *b* and *c*, the branching ratios of reactions (b) and (c), should be zero for $1s$. This unrealistically large value indicates residual errors in the dissociative multiple ionization efficiency estimates.

from the ion yield spectra (Figs. 6 and 7) after background subtraction. Thus they represent our best estimates for the ion production following each of the electronic processes, although a relatively large uncertainty is associated with the less populated reaction pathways (see footnote e of Table IV); this uncertainty arises largely in the estimate of η for which it is difficult to provide quantitative error estimates.

From this analysis one observes that the ionic fragmentation pathways are remarkably *insensitive to the location of the core hole.* In contrast, very large differences are observed among the valence υ,π^* resonances and $1s$ ionization, consistent with the known substantial differences in their electronic decay processes. In addition there are smaller but significant differences between the C $1s$ and O $1s\pi^*$ resonances in the contributions of reactions producing C^+, O^+, and $(C^+ + O^+)$. Our results for $1s$ ionization are discussed in relation to the Auger electron and Auger-ion coincidence spectra in Sec. IV A while the fragmentation following autoionization of the $1s \rightarrow \pi^*$ states is discussed in Sec. IV B.

IV. DISCUSSION

A. 1*s* continua — Auger processes

$(C^+ + O^+)$ production dominates both core ionization continua and thus we first focus attention on the coupling of the $1s$ ion states with the CO^{2+} dissociative curves. Some of the potential curves relevant to the Auger decay processes giving rise to the energetic $(C^+ + O^+)$ ion pairs are plotted in Fig. 13. The $1s$ potential curves were taken from the calculations of Correia *et al.*[9] while a selection of the results of Wetmore *et al.*[19] have been adopted for the dissociative CO^{2+} curves leading to $C^+ + O^+$. As indicated by the arrows in the figure, if one assumes that autoionization occurs on a much shorter time scale than dissociation, the difference in energy between the dissociative potential curve in the Franck-Condon region (i.e., at the equilibrium geometry of ground-state CO, $1.08 < R < 1.18$ Å) and the relevant $C^+ + O^+$ dissociation limit determines the kinetic energy released to the ion pair. Although there are many more CO^{2+} states in this energy region, we have selected representative states which match the main Auger electron energies and which give predicted ion kinetic energies close to the maxima in the KERD's determined from the weak-field PIPICO. This approach is somewhat arbitrary and relies on assumptions (absence of curve crossing, system deposited on the Franck-Condon part of the CO^{2+} potential curves, . . .) that need to be tested. Comparison with the direct observation of the CO^{2+} states formed at threshold is essential and is in progress.[57,59]

Of the 11 states specified in detail by Wetmore *et al.*,[19] only the lowest-energy states of $^3\Pi$ and $^3\Sigma^-$ symmetry (2 and 3 in Fig. 13), decay to the lowest-energy $C^+(^2P) + O^+(^4S)$ limit, in which both fragment ions are found in their ground states. The ion kinetic energies released in vertical transitions to these curves are 5.0 and 7.4 eV according to the Wetmore *et al.* calculations[19] (see Table V). According to the KERD's derived from the weak-field PIPICO, there are very few events which produce ion pairs with less than 7.5 eV in the $1s$ continua. Thus the combination of our results and the CO^{2+} calculations indicate that, in the absence of curve crossings, the $1s$ states decay predominantly to excited C^+ and/or O^+, particularly to the $C^+(^2P) + O^+(^2D)$ limit (B) which lies 3.3 eV above the lowest $C^+(^2P) + O^+(^4S)$ limit (A). Most excited O^+ states are metastable with very long

TABLE V. $(C^+ + O^+)$ ion kinetic energy releases predicted from calculated CO^{2+} curves.

state	BE[a] (eV)	limit[b]	KER[c] (eV)	width[d] (eV)
$^1\Sigma^+ - 1$	41.9	B	2.7	0.2
$^1\Pi$	41.6	B	2.3	0.2
$^3\Pi$	41.0	A	5.0	0.2
$^3\Sigma^-$	43.4	A	7.4	3.0
$^1\Sigma^+ - 2$	48.4	C	7.4	1.4
$^1\Delta$	47.0	B	7.7	2.5
$^3\Sigma^+$	48.7	B	9.4	0.6
$^3\Delta$	49.9	B	10.6	2.0
$^1\Sigma^-$	51.1	B	11.8	1.0
$^1\Sigma^+ - 3$	58.6	C	17.6	1.2
$^1\Sigma^+ - 4$	60.4	D	19.1	1.0

[a]Binding energies (BE) refer to the energy of the CO^{2+} state at the equilibrium geometry of ground-state CO. They are determined by adding 35.4 eV to the energies given by Wetmore *et al.* (Ref. 19).

[b]The symmetries and energies (eV, relative to the $v=0$ level of the CO ground state) of $(C^+ + O^+)$ limits are

A: $C^+(^2P)+O^+(^4S)$, 36.0; B: $C^+(^2P)+O^+(^2D)$, 39.3;
C: $C^+(^2P)+O^+(^2P)$, 41.0; D: $C^+(^4P)+O^+(^4S)$, 41.3;
E: $C^+(^4P)+O^+(^2D)$, 44.6 .

[c]The mean value of the kinetic energy release (KER) is given by the difference between the vertical binding energy and the atomic ion limits.

[d]The widths are the differences in the potential curves at the CO ground-state Franck-Condon turning points (1.08 and 1.18 Å).

($\simeq 10^3 - 10^4$ s) radiative lifetimes and therefore do not give rise to experimentally detectable fluorescence. Nevertheless, the $O^+(^4S)$ state can be distinguished from the $O^+(^2D)$ state by their specific reactivity with neutral molecules. According to recent studies of $O^+ + N_2$ reactions,[60,61] the ^4S state of O^+ produces NO^+ whereas the ^2D state of O^+ gives N_2^+. Thus photoionization mass spectrometry of CO-N_2 mixtures may provide a means to demonstrate the copious excited O^+ production which is expected from the comparison of our KERD's and the calculated CO^{2+} potential curves.

A rather important secondary channel in the C 1*s* and O 1*s* continua is dissociative triple ionization producing $(C^{2+} + O^+)$. According to our analysis (Table IV) about half of the C^{2+} produced at the σ^* resonances in the 1*s* continua arises from this process. According to the Auger-ion coincidence measurements,[23] C^{2+} production only occurs for states with binding energies above 58 eV in the O 1*s* Auger decay (corresponding to the spectrum taken at point *D* in Fig. 7 of Ref. 23). From the relative intensity of *D* ($\simeq 10\%$ of all O 1*s* Auger) it would appear that this state by itself could explain the 7% contribution of $C^{2+} + O$ [reaction (e)] that we observe. It is only Auger decay to states of higher binding energies (> 65 eV) that can produce the $(C^{2+} + O^+)$ ion pairs. This is consistent with the increase in the sum of the C^{2+} and O^+ kinetic energies observed on going from *D* (Auger energy of 58 eV) to *E* (Auger energy of 72 eV). It is also consistent with the thermodynamic threshold for $(C^{2+} + O^+)$ production [$\simeq 47$ eV (Refs. 18 and 62)] and the large exothermicity of the fragmentation (Table III). In the C 1*s* continuum, a similar pattern emerges, with the CO^{2+} states at 48 and 62 eV binding energy (points *C* and *D* in Fig. 7 of Ref. 23) dissociating to produce $(C^{2+} + O)$ and the higher-energy states such as *E* ($\simeq 72$ eV) producing $(C^{2+} + O^+)$ pairs. An increase in the sum of the C^{2+} and O^+ kinetic energies is also observed on going from *D* to *E* in the C 1*s* Auger-ion coincidence measurements.[23]

B. $1s \rightarrow \pi^*$ resonances—autoionization

There is a large yield of single ionization [processes (a), (b), and (c)] and a relatively low yield (20–25%) of $(C^+ + O^+)$ pairs at both $1s \rightarrow \pi^*$ resonances. This is a surprising observation since it is opposite to the situation found in Xe (Refs. 15 and 63) and Kr (Ref. 63) atoms and in different molecules, like $Si(CH_3)_4$ (Ref. 4) or CH_3Br,[7] where the decay of resonances below the first inner-shell ionization threshold efficiently results in double ionization. On this point the CO situation is rather similar to argon.[63] The ion yield at the C $1s \rightarrow \pi^*$ resonance in CO can be explained with the aid of the deexcitation electron spectrum (DES) of Eberhardt *et al.*[22] reproduced in Fig. 14. This spectrum is divided into three zones: the normal autoionization processes leading to stable CO^+ show up in region I, while those leading to dissociative CO^+ states producing $(C^+ + O)$ or $(C + O^+)$ contribute to region II. In the third region, delimited by the CO^{2+} threshold around 41.5 eV,[62,64] deexcitation to the double ionization continuum is energetically possible. The relative preponderance of zones I and II over zone III has the consequence that single ionization dominates at the $1s \rightarrow \pi^*$ resonances. The potential curves involved in the decay at the $1s \rightarrow \pi^*$ resonances are represented only schematically in Fig. 14, since little information is available on them[65] or on the spectroscopy of the dissociative excited CO^- states.[62,66,67]

The quantitative details of the C 1*s* (Refs. 18, 20, 21, and 22) autoionization electron spectrum recorded at the π^* resonances are consistent with our ionization reaction yields, as outlined below. The DES spectrum shows peaks arising from electronic decay in which the π^* electron either participates or remains a spectator. The participator processes include decay to the stable $\underline{5\sigma}$, $\underline{1\pi}$, and $\underline{4\sigma}$ states of CO^+ [peaks 1–3 with $\simeq 17\%$ of total intensity, as measured from integration of the published DES (Ref. 22)] as well as to the dissociative $\underline{3\sigma}$ state of CO^+ (peak 4 with $\simeq 10\%$ of the total intensity). The spectator processes involve decay to two hole-one particle ($2h$-$1p$) states and produce five prominent peaks, labeled ($D1$–$D5$) by Eberhardt *et al.*[22] Of the latter, $D1$–$D3$ ($\simeq 42\%$) have binding energies below 41 eV (the effective onset for CO^{2+} production) while $D4$ and $D5$ ($\simeq 31\%$) have binding energies above 41 eV.

The 17% yield of stable CO^+ states (region I, Fig. 14) is in reasonable agreement with our observation of a 9% contribution to reaction (a), that of CO^+ production (Table IV), if we take into account the relatively large un-

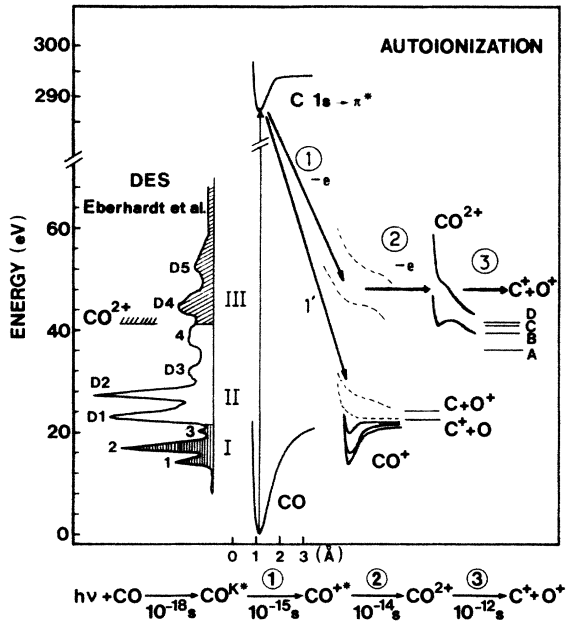

FIG. 14. Schematic of the autoionization of the C $1s\pi^*$ state, including the postulated two-step autoionization producing $(C^+ + O^+)$. The experimental autoionization spectrum is taken from Eberhart *et al.* (Ref. 22). Features 1–4 correspond to participator decay to the $\tilde{X}^2\Sigma$, $A^2\Pi$, $\tilde{B}^2\Sigma$, and $\tilde{C}$ states of CO^+. Features $D1$–$D5$ are spectator decay to $2h$-$1p$ states (see Refs. 22 and 24 for dominant configurations). The CO^+ potential curves in dashed lines are hypothetical, while solid lines are used for the calculated ground-state, C $1s\pi^*$, CO^+ (Ref. 9), and CO^{2+} (Ref. 19) potential curves. The scheme at the bottom represents the sequence of events leading to $(C^+ + O^+)$ along with suggested, characteristic time scales. According to our analysis only CO^+ is produced in region I, primarily $(C^+ + O)$, with some $(C + O^+)$ in region II, and predominantly $(C^+ + O^+)$ in region III of the autoionization of the C $1s \rightarrow \pi^*$ state.

certainties associated with our branching ratios, and with the integration of Eberardt's deexcitation spectrum. The intensity in region III, above 41 eV binding energy, amounts to 31% of the total autoionization signal. This is quite similar to our estimate of a 25% contribution of $(C^+ + O^+)$ pair production at the C $1s \rightarrow \pi^*$ resonance, CO^{2+} states with dissociative curves leading to $C^+ + O^+$ (see Fig. 14). The processes involved here include double resonant Auger (two electrons ejected simultaneously with a continuous kinetic energy distribution of each electron) or two-step autoionization (two electrons ejected sequentially, each with well-defined kinetic energies);[68] since the C $1s$ autoionization spectrum exhibits rather well-defined bands ($D4$,$D5$) we favor the two-step autoionization picture for $(C^+ + O^+)$ production, as depicted schematically in Fig. 14.

According to Table IV, the $(C^+ + O)$ final ion state is populated in 44% of the decays of C $1s\pi^*$, while the $(C + O^+)$ final state contributes only 12%. The strong preference for production of C^+ at the C $1s\pi^*$ state must arise in the dissociation of the CO^+ states corresponding to peaks $D1$, $D2$, $D3$, and/or 4 (3σ) which represent 17, 18, 7, and 10% of the total autoionization, respectively (region II, Fig. 14). $D1$ is assigned to the $[(5\sigma\, 5\sigma\, 2\pi), (5\sigma\, 1\pi\, 2\pi)]$, while $D2$ is assigned to the $[(4\sigma\, 5\sigma\, 2\pi), (5\sigma\, 1\pi\, 2\pi)]$ configurations.[22,24] On the basis of binding energies, the $D1$ and $D2$ $2h$-$1p$ satellites are identical to the $\tilde{C}$ and $\tilde{D}$ states identified in valence ionization studies of CO^+.[69] The $\tilde{C}$ state (and thus $D1$) is known to predissociate exclusively to $(C^+ + O)$, whereas the $\tilde{D}$ state ($D2$) decays to both $(C^+ + O)$ and $(C + O^+)$, as do the valence ionized states at energies corresponding to $D3$ and 4 (labeled $\tilde{G}$ and O $2s$ in Ref. 69).[64,69–71] The branching ratios deduced for $(C^+ + O)$ and $(C + O^+)$ production of each of these states from $(e,e + \text{ion})$ and $(e,2e)$ experiments,[69] as well as the relative areas of the DES peaks predict a $(C^+ + O)$ yield of 35% and a $(C + O^+)$ contribution of 17%. This is in reasonable agreement with the 44% contribution of process (b) producing C^+, and 12% contribution of process (c) producing O^+, deduced from the present measurements (Table IV).

We note that the C^+ and O^+ yields were approximately equal when measured in coincidence with the autoionization lines using broadband 300-eV photoionization spectrum A of Fig. 8 of Ref. 23. Although the majority of the electron signals at A arise from autoionization of the C $1s\pi^*$ state, the equal C^+ and O^+ Auger-ion coincidence yield is not necessarily inconsistent with our observation of a large excess of C^+ production at the C $1s \rightarrow \pi^*$ resonance because of the smearing of the Auger electron energy scale by the ion extraction field, which mixes in the normal C $1s$ Auger processes, dominated by $(C^+ + O^+)$. Our 287-eV PIPICO measurements confirm the suggestion of Eberhardt *et al.*[23] that a portion (25%) of the C^+ and O^+ signal they see at A arises from decay to $(C^+ + O^+)$ of the C $1s\pi^*$ state, populated by the low-energy wings of the 300-eV undulator radiation.

C. Comparison of ion yields from photoionization of gas, solid, and chemisorbed CO

The photon-stimulated ion desorption spectra (PSID) of surfaces in the region of core excitation frequently closely resemble the corresponding photoabsorption spectra. Thus, for example, the O^+ yield from MgO surfaces reproduces all details of the O $1s$ spectrum of MgO.[72] This has been explained by Knotek and Feibelman (KF)[73] in terms of Auger decay to dissociative two-hole states which produce ions with sufficient energy to escape the surface before reneutralization. The KF model appears to be particularly applicable to ionic materials but it is also frequently proposed as a general model for ion desorption of chemisorbed molecules by high-energy electron or x-ray photon impact. However, for CO and NO on Ni(100),[29,30] CO on Cu(100),[31] and CO and NO on Ru(100),[32] the O^+ yield spectrum in the inner-shell regions of the CO or NO molecules exhibits an almost complete quenching of the "discrete" excitation structure and suppression of the near continuum such that the major onset of O^+ ion desorption is 20–30 eV higher than that in the corresponding $1s$ photoabsorption spectrum of the isolated molecule. The absence of desorption signal in the near-edge region has been explained[30,31,75] in terms of

efficient reneutralization of normal core-excited and core-ionized one-electron states of the molecule through charge transfer from the metal substrate. The delayed onset of the O^+ desorption signal is then associated with the opening of secondary, high-energy multielectron excitation channels[75] which decay to valence states with three or more valence holes. These shake-up and shake-off states are not as effectively relaxed by charge transfer from the metal and thus fragmentation and ion desorption can occur before reneutralization.

Comparison of the present O 1*s* results to those for the photodissociation of CO adsorbed on metal surfaces[29–31] confirms that the delayed onset of O^+ production is a surface-specific effect. Our results also provide further insight into the multielectron mechanism. The 560-eV threshold for the deviation between the shapes of the O^{2+} and C^{2+} partial yield spectra and that of the total ion yield spectrum (Fig. 7) is identical to the location of the rapid onset of O^+ desorption[29–32] and to the shake-off threshold in x-ray photoemission spectroscopy (XPS) of free and chemisorbed CO.[74] Thus the multielectron states giving rise to increased yields of O^{2+}, and probably $(C^{2+}+O^+)$, in free CO above 560 eV could be the same as those leading to O^+ PSID in chemisorbed CO. Furthermore, Jaeger *et al.*[29,30] suggested that multielectron states in the C 1*s* continuum are much weaker than in the O 1*s* continuum in order to explain the weak[29,30] or absent[31,32] O^+ desorption in the C *K* shell. Our results support this speculation in that the deviation from the total ion yield curve is much less in the carbon *K*- shell O^{2+} partial ion yield spectrum (although similar in the C^{2+} channel) (Fig. 6). We note that there is considerable disagreement as to the identity of the multielectron process(es) active in PSID. Jaeger *et al.*[29,30] argue in favor of (O $\underline{1s}3\sigma$). Although this is supported by Ramaker's calculations,[75] it does not seem consistent with the present gas phase results, if one assumes that the enhanced O^{2+} and/or C^{2+} yields in free CO correspond to signals from states leading to O^+ PSID. This is because the threshold for (O $\underline{1s}3\sigma$) shake off will be above 580 eV [IP(O 1*s*)=542, IP(3σ)=39 eV plus correlation energy, where IP stands for ionization potential]. [We note that the additional increase in the O^{2+} curve above 580 eV (Refs. 29 and 30) is likely from (O $\underline{1s}3\sigma$) shake off.] The proposal of Treichler *et al.*[31,32] for (O $\underline{1s}5\sigma$) shake off is in better agreement with the 560-eV threshold for enhanced O^{2+} production in free CO since IP(5σ)=14 eV.

If reneutralization is not selective one might expect the A^+ yield from PSID (where *A* represents any atomic fragment) to be proportional to the A^{2+} yield in the free molecule. However, the higher yield of C^{2+} than O^{2+} and the greater contributions of $(C^{2+}+O^+)$ production from shake off that we observe in free CO contrasts with the relatively greater yields of O^+ than C^+ in PSID of chemisorbed CO.[30,31] This suggests that the intrinsic intramolecular decay processes are not directly reflected in the PSID yields. The reversal of the O^+-C^+ yields in PSID relative to their proposed $(C^+ + O^{2+})$ and $(C^{2+}+O^+)$ precursors[31] may be related to a lower rate of reneutralization of O^{2+} than C^{2+} hole states by the metal substrate, since the substrate is farther from the O than the C atom in CO bonded carbon end down. Alternatively, the O^+ PSID could arise from the $(C^{2+}+O^+)$ dissociative triple ionization, in which case the relative C^{2+} yields would be the appropriate monitor since the O^+ signal from multielectron processes will be difficult to determine against the large O^+ yield from the dominant $(C^+ + O^+)$ production. Again this hypothesis leads to inconsistencies between the gas and surface results since the C^{2+} signal is seen in both the C 1*s* and O 1*s* regions, whereas O^+ PSID is only found above the O 1*s* edge. As with the first hypothesis, preferential reneutralization at the carbon end could provide a means of reconciling the observations for ion yields from gas and chemisorbed CO. Finally, for CO bonded carbon end down perpendicular to the surface, the initial C^+ (or C^{2+}) trajectory in Coulomb explosions of CO^+ or CO^{2+} will be into the surface. This means that it is very unlikely that a C^+ ion can escape before reneutralization.

Treichler *et al.*[31] observe relatively large yields of CO^+ from CO/Ru(100) [and NO^+ from NO/Ru(100) (Ref. 32)] which follow the excitation spectra, including the 1*s* continuum shape. Since there is negligible CO^+ production in either the C 1*s* or the O 1*s* continuum of free CO (Figs. 6 and 7), this signal must arise indirectly through surface modifications of the dissociative double ionization processes which dominate the decay of the $\underline{1s}$ states of the free molecule. The weak C^+ and O^{2+} PSID from O 1*s* photoionization of CO/Ru(100) (Ref. 31) are very similar to each other and exhibit the same delayed onset (560 eV) as O^+ PSID, indicating that they arise primarily from shake-off processes. In contrast, a small O^+ signal is observed below 560 eV (Refs. 29-31) which is associated with $(C^+ + O^+)$ events which are incompletely reneutralized.

In their studies of the photodesorption of solid CO Rosenberg *et al.*[36] observed that C^+ and O^+ production dominates at all energies, with the only other ions reported being CO^+, C_2O^+, and $(CO)_2^+$, all with yields less than 10% of that of O^+. The absence of C^{2+} and O^{2+} PSID signals[36] suggests that there may be reneutralization processes in the solid similar to those in chemisorbed CO on metals[29–31] since C^{2+} and O^{2+} are observed with significant yields in the 1*s* continua of the free molecule. The $I(C^+)/I(O^+)$ ratio in both the C 1*s* and O 1*s* regions of the PSID of solid CO is between 3.8 and 4.6. This is much larger than the 0.9 to 1.7 $I(C^+)/I(O^+)$ ratios we observe for photofragmentation of CO in the gas phase. Kinetic energy discrimination by the TOF analyzer used for the PSID measurements[36] cannot explain the larger $I(C^+)/I(O^+)$ ratios in the solid since, if present, it would artificially *reduce* the $I(C^+)/I(O^+)$ ratio because of higher discrimination against the faster C^+ ion (see Fig. 3). Thus, both the types of ions produced and the modified $I(C^+)/I(O^+)$ ratio provide clear evidence that ionic fragmentation following core excitation differs between solid and gaseous CO. We suggest that the differences between the solid and gas $I(C^+)/I(O^+)$ ratios are related to greater C^+ than O^+ mobility in a matrix of solid CO and thus a higher C^+ escape probability, rather than arising from a fundamental difference in the initial electronic excitation

or intramolecular relaxation between the free molecule and the weakly interacting van der Waals solid. The $I(C^+)/I(O^+)$ ratio curves from the PSID of the solid show prominent peaks at both π^* resonances,[36] exactly as observed for free CO (Figs. 8 and 9). Thus, although there is modification of the gas phase ion yields, possibly from the preferential mobility of C^+, the enhanced C^+ production at the π^* resonances persists through the details of the ion escape.

D. Comments on site- and state-selective processes in the decay of inner-shell states

From Table IV and the similarity of Figs. 8 and 9, it is clear that the ionic fragmentation of CO following core excitation and ionization is not particularly site selective. This suggests several comments in relation to recent reports on this subject.[1-6] Obviously in a diatomic molecule, in which only one bond can be broken, the only selective aspect could be the number of positive charges on the atomic fragments. In both the C 1*s* and O 1*s* spectra of CO, C^{2+} and O^{2+} are found with only small intensities and are produced in a ratio of 2.7(5) at all energies outside of the π^* resonances. In contrast, the main decay channel is $(C^+ + O^+)$, independent of the location of the initial excitation. The decoupling of the initial, localized core excitation from the observed ion yields arises because, irrespective of the site of the core hole, the electronic decay produces *the same multihole valence states,* which by nature are "spread" over the whole molecule. Moreover, in the case of the π^* bound resonance, the excited electron is in an antibonding C-O orbital which also "smears out" the core-hole localization. However, there is a dramatic difference between the core resonances and the underlying valence ionization continuum. Indeed direct single ionization is not as efficient as core resonant photoionization at producing fragmentation, which is why the CO^+ yield is relatively much larger around 280 eV than at higher energies (Fig. 8).

In larger molecules, the same effects will occur, except that more "big" fragments will be produced in valence than core ionization. This is indeed what has been found in acetone near the C 1*s* edge.[1,5] Consequently, the site selectivity of fragmentation following core excitation, which is of great interest for large polyatomics, is still an open question. So far the available results suggest that the electronic relaxation pathways are not generally selective.[1-8] This may not be true in cases where a core-to-bound resonance dissociates rapidly, before autoionization or resonant Auger[7] decay occurs, or in very big molecules in which the damage around the core-excited atom is kept at a distance significantly smaller than the overall size of the molecule.

ACKNOWLEDGMENTS

We thank the staff of the Laboratoire pour l'Utilisation du Rayonnement Electromagnétique for their expert operation of the ACO storage ring, as well as J. Delwiche and M. J. Hubin-Franskin for constructing the analyzers used in these experiments. A.P.H. acknowledges financial support from Natural Science and Engineering Research Council (NSERC). The Laboratoire pour l'Utilisation du Rayonnement Electromagnétique is Laboratoire associé au Centre National de la Recherche Scientifique, au Commissariat à l'Energie Atomique et au Ministère de l'Education Nationale.

*Permanent address: Department of Chemistry, McMaster University, Hamilton, Ontario, Canada L8S 4MI.

†Also at Département de Physico-chimie, CEA, Centre d'Etudes Nucléaires de Saclay, 91191, Gif-sur-Yvette Cédex, France.

[1]W. Eberhardt, T. K. Sham, R. Carr, S. Krummacher, M. Strongin, S. L. Weng, and D. Wesner, Phys. Rev. Lett. **50**, 1038 (1983).

[2]W. Eberhardt and T. K. Sham, Proc. SPIE **447**, 143 (1984).

[3]K. Müller-Dethlefs, M. Sander, L. A. Chewter, and E. W. Schlag, J. Phys. Chem. **88**, 6098 (1984).

[4]P. Morin, G. G. B. de Souza, I. Nenner, and P. Lablanquie, Phys. Rev. Lett. **56**, 131 (1986).

[5]M. C. Nelson, J. Murakami, S. L. Anderson, and D. M. Hanson, J. Chem. Phys. **86**, 4442 (1987).

[6]I. Nenner and A. Beswick, *Handbook on Synchrotron Radiation,* edited by G. V. Marr (North-Holland, Amsterdam, 1987), Vol. II, Chap. 6.

[7]I. Nenner, P. Morin, M. Simon, P. Lablanquie and G. G. B. de Souza, *Proceedings of DIET III, New York, 1987* edited by M. Knotek and R. Stulhen (Springer-Verlag, New York, in press). (DIET is an acronym for ion desorption induced by electronic transitions.)

[8]A. P. Hitchcock, P. Morin, M. Simon, P. Lablanquie, and I. Nenner (to be published).

[9]N. Correia, A. Flores-Riveros, H. Ågren, K. Helenelund, L. Asplund, and U. Gelius, J. Chem. Phys. **83**, 2035 (1985).

[10]P. Morin and I. Nenner, Phys. Rev. Lett. **56**, 1913 (1986).

[11]G. G. B. de Souza, P. Morin, and I. Nenner, Phys. Rev. A **34**, 4770 (1986).

[12]T. X. Carroll, S. E. Anderson, L. Ungier, and T. D. Thomas, Phys. Rev. Lett. **58**, 867 (1987).

[13]T. X. Carroll and T. D. Thomas, J. Chem. Phys. **86**, 5221 (1987).

[14]T. A. Carlson and R. M. White, J. Chem. Phys. **44**, 4510 (1966).

[15]J. H. D. Eland, S. Wort, P. Lablanquie, and I. Nenner, Z. Phys. D **4**, 31 (1986).

[16]T. A. Carlson and M. O. Krause, J. Chem. Phys. **56**, 3206 (1972).

[17]R. B. Kay, P. E. Van der Leeuw, and M. J. Van der Wiel, J. Phys. B **10**, 2521 (1977).

[18]W. Eberhardt, C. T. Chen, W. K. Ford, E. W. Plummer, and H. R. Moser, *Proceedings of DIET II, Schloss Elman, 1984,* edited by W. Brenig and D. Menzel (Springer-Verlag, Berlin, 1985), p. 50.

[19]R. W. Wetmore, R. J. LeRoy, and R. K. Boyd, J. Phys. Chem. **88**, 6318 (1984).

[20]L. Ungier and T. D. Thomas, Chem. Phys. Lett. **96**, 247 (1983).

[21]L. Ungier and T. D. Thomas, Phys. Rev. Lett. **53**, 435 (1984).

[22]W. Eberhardt, E. W. Plummer, C. T. Chen, and W. K. Ford, Aust. J. Phys. **39**, 853 (1986).

[23]W. Eberhardt, E. W. Plummer, I. W. Lyao, R. Reininger, R.

Carr, W. K. Ford, and D. Sondericker, Aust. J. Phys. **39**, 633 (1986).
[24]H.-J. Freund and C.-M. Liegener, Chem. Phys. Lett. **134**, 70 (1987).
[25]U. Gelius, E. Basilier, S. Svensson, T. Bergmark, and K. Siegbahn, J. Electron Spectrosc. **2**, 405 (1974).
[26]A. Flores-Riveros, N. Correia, H. Ågren, L. Pettersson, M. Bäckström, and J. Nordgren, J. Chem. Phys. **83**, 2053 (1985).
[27]M. Tronc, G. C. King, and F. H. Read, J. Phys. B **12**, 137 (1979).
[28]A. P. Hitchcock and C. E. Brion, J. Electron Spectr. **18**, 1 (1980).
[29]R. Jaeger, J. Stöhr, R. Treichler, and K. Baberschke, Phys. Rev. Lett. **47**, 1300 (1981).
[30]R. Jaeger, R. Treichler, and J. Stöhr, Surf. Sci. **117**, 533 (1982).
[31]R. Treichler, W. Riedl, W. Wurth, P. Feulner, and D. Menzel, Phys. Rev. Lett. **54**, 462 (1985).
[32]R. Treichler, W. Riedl, W. Wurth, P. Feulner, and D. Menzel, *Proceedings of DIET II, Schloss Elman, 1984,* edited by W. Brenig and D. Menzel (Springer-Verlag, Berlin, 1985), p. 68.
[33]M. J. Van der Wiel and Th. M. El-Sherbini, Physica (Utrecht) **59**, 453 (1972).
[34]A. P. Hitchcock and C. E. Brion (e,e + ion) results (unpublished).
[35]Y. Sato, A. Yagishita, T. Nagata, T. Hayaishi, M. Yoshino, T. Koizumi, Y. Itoh, T. Matsuo, H. Shibata, and T. Sasaki, Koo Energi Kenkyushoo Progress Report No. 4, 1986 (unpublished).
[36]R. A. Rosenberg, P. J. Love, P. R. LaRoe, V. Rehn, and C. C. Parks, Phys. Rev. B **31**, 2634 (1985).
[37]F. J. Himpsel, Y. Jugnet, D. E. Eastman, J. J. Domelon, D. Grimm, G. Landgren, A. Marx, J. F. Morar, R. A. Pollak, and J. Schneir, Nucl. Instrum. Methods **222**, 107 (1984).
[38]R. N. S. Sodhi and C. E. Brion, J. Electron Spectrosc. **34**, 363 (1984).
[39]D. Arvanitis, U. Döbler, L. Wenzel, K. Baberschke, and J. Stöhr, Surf. Sci. **171**, 686 (1986).
[40]A. P. Lukirskii and T. M. Zimkina, Izv. Akad. Nauk SSSR Ser. Fiz. **27**, 817 (1963) [Bull. Acad. Sci. USSR Phys. Ser. **27**, 808 (1963)].
[41]P. Lablanquie, I. Nenner, P. Millie, P. Morin, J. H. D. Eland, M. J. Hubin Franskin, and J. Delwiche, J. Chem. Phys. **82**, 2951 (1985).
[42]G. Doolan and D. Liberman, Phys. Scr. (to be published).
[43]R. B. Kay, P. E. Van der Leeuw, and M. J. Van der Wiel, J. Phys. B **10**, 2513 (1977).
[44]R. McLaren, S. A. C. Clark, I. Ishii, and A. P. Hitchcock, Phys. Rev. A **36**, 1683 (1987).
[45]E. H. A. Granneman and M. J. Van der Wiel, in *Handbook on Synchrotron Radiation,* edited by E. E. Koch (North-Holland, Amsterdam, 1983), Vol. 1, p. 367.
[46]A. P. Hitchcock, C. E. Brion, and M. J. Van der Wiel, J. Phys. B **11**, 3245 (1978).
[47]A. P. Hitchcock, C. E. Brion, and M. J. Van der Wiel, Chem. Phys. Lett. **66**, 213 (1979).
[48]J. L. Dehmer, A. C. Parr, and S. H. Southworth, in *Handbook on Synchrotron Radiation,* edited by G. V. Marr (North-Holland, Amsterdam, 1987), Vol. II.
[49]J. Stöhr, R. Jaeger, and J. J. Rehr, Phys. Rev. Lett. **51**, 821 (1983).
[50]T. D. Thomas, J. Electron Spectrosc. **40**, 259 (1986).
[51]C. M. Truesdale, D. W. Lindle, P. H. Kobrin, U. E. Becker, H. G. Kerkoff, P. A. Heimann, T. A. Ferrett, and D. A. Shirley, J. Chem. Phys. **80**, 2319 (1984).
[52]D. M. Barrus, R. L. Blake, A. J. Burek, K. C. Chambers, and A. L. Pregenzer, Phys. Rev. A **20**, 1045 (1979).
[53]A. Reimer, J. Schirmer, A. M. Bradshaw, U. Becker, H. G. Kerkhoff, B. Langler, D. Szostak, R. Wehlitz, and W. Braun, Phys. Rev. Lett. **57**, 1707 (1986).
[54]B. Brehm and G. De Frênes, Int. J. Mass. Spectrom. Ion Phys. **26**, 251 (1978).
[55]J. H. Beynon, R. M. Caprioli, and J. W. Richardson, J. Am. Chem. Soc. **93**, 1852 (1971).
[56]J. M. Curtis and R. K. Boyd, J. Chem. Phys. **80**, 1150 (1984).
[57]P. Lablanquie, J. Delwiche, M. J. Hubin-Franskin, I. Nenner, J. H. D. Eland, and K. Ito, J. Mol. Struct. (to be published).
[58]D. Cossart (private communication).
[59]P. Fournier (private communication).
[60]J. Glosik, A. B. Rashit, N. D. Twiddy, N. G. Adams, and D. Smith, J. Phys. B **11**, 3365 (1978).
[61]J. D. Burley, K. M. Ervin, and B. Armentrout, J. Chem. Phys. **86**, 1944 (1987).
[62]T. Masuoka, J. Chem. Phys. **82**, 3921 (1985).
[63]T. Hayaishi, Y. Morioka, Y. Kageyama, M. Watanabe, J. H. Suzuki, A. Mikuni, G. Isoyama, S. Asaoka, and M. Nakamura, J. Phys. B **17**, 3511 (1984).
[64]A. S. Newton and A. F. Sciamanna, J. Chem. Phys. **53**, 132 (1970).
[65]J. Marchand, J. D'Ivan, and J. Janin, Spectrochim. Acta Part A **25**, 605 (1969).
[66]F. Guérin, Theor. Chim. Acta (Berlin) **17**, 97 (1970).
[67]R. Locht and J. M. Dürer, Chem. Phys. Lett. **34**, 508 (1975).
[68]P. Morin, in *Giant Resonances in Atoms, Molecules and Solids,* Vol. 151 of *NATO Advanced Study Institute, Series B: Physics,* edited by J. P. Connerade, J. M. Esteva, and R. C. Karnatak (Plenum, New York, 1987), p. 291.
[69]G. R. Wight, M. J. Van der Wiel, and C. E. Brion, J. Phys. B **9**, 675 (1976).
[70]T. Masuoka and J. A. R. Samson, J. Chem. Phys. **74**, 1093 (1981).
[71]K. Ito, A. Yagashita, T. Hayaishi, and Y. Morioka, J. Phys. B **19**, 3061 (1986).
[72]R. L. Kurtz, R. Stockbauer, R. Nyholm, S. A. Flodström, and F. Serf, Phys. Rev. B **35**, 7794 (1987).
[73]M. L. Knotek and P. J. Feibelman, Phys. Rev. Lett. **40**, 964 (1978).
[74]E. W. Plummer, C. T. Chen, W. K. Ford, W. Eberhardt, R. P. Messmer, and H.-J. Freund, Surf. Sci. **158**, 58 (1985); J. Schirmer, G. Angonoa, S. Svensson, D. Nordfors, and U. Gelius, J. Phys. B **20**, 6031 (1987).
[75]D. E. Ramaker, J. Chem. Phys. **78**, 2998 (1983).